Economic Geology, v. 102, pp. 3–26

U-Pb and Re-Os Geochronologic Evidence for Two Alkalic Porphyry Ore-Forming Events in the Cadia District, New South Wales, Australia

Alan J. Wilson,[†,*] David R. Cooke,

Centre for Excellence in Ore Deposits, University of Tasmania, Private Bag 79, Hobart, Tasmania 7001, Australia

Holly J. Stein,

AIRIE Program, Colorado State University, Fort Collins, Colorado, and Geological Survey of Norway, 7491 Trondheim, Norway

C. Mark Fanning,

Research School of Earth Sciences, Australian National University, Canberra, ACT 0200, Australia

John R. Holliday, and Ian J. Tedder

Newcrest Mining Limited, Cadia Road, Orange, New South Wales 2800, Australia

Abstract

The Cadia district, located in the eastern Lachlan fold belt of New South Wales, Australia, comprises four gold-copper porphyry deposits (Ridgeway, Cadia Quarry, Cadia Hill, and Cadia East) and two related iron-copper-gold skarn deposits (Big Cadia and Little Cadia). These deposits formed along a northwest-striking, arc-transverse structural corridor within the intraoceanic Macquarie arc. This arc is composed of a belt of Early Ordovician to Early Silurian mafic to intermediate volcanic, volcaniclastic, and intrusive rocks of calc-alkalic to alkalic composition. The Cadia porphyry deposits are temporally and genetically associated with composite intrusive complexes of alkalic monzodiorite to quartz monzonite.

U-Pb dating of igneous minerals from the intrusions and Re-Os dating of hydrothermal molybdenite from the deposits has revealed the presence of two temporally discrete events of magmatism and related porphyry-style mineralization in the Cadia district. The monzonitic intrusive complex related to mineralization at Ridgeway and a quartz monzonite porphyry stock that lies immediately southwest of the Cadia Quarry deposit are early Late Ordovician (456–454 Ma). In contrast, the quartz monzonite porphyry stock that hosts the Cadia Quarry and Cadia Hill orebodies and an intermineral quartz monzonite porphyry dike at Cadia East are Early Silurian (~438 Ma). Re-Os molybdenite ages determined for quartz-sulfide veins within the early Late Ordovician quartz monzonite porphyry confirm multiple episodes of mineralization associated with the Cadia Quarry deposit, suggesting a complex history between 460 and 450 Ma. At Cadia Hill, Cadia Quarry, and Cadia East, a widespread event of porphyry gold-copper mineralization is recorded at about 443 to 441 Ma, based on three Re-Os molybdenite ages from sheeted quartz sulfide veins. Similar ages for magmatic zircon from the host intrusions support a link between dated intrusions and mineralization.

These new ages are in general agreement with the ages of other porphyry gold-copper and related epithermal deposits of the Eastern Lachlan fold belt and help to constrain the relationship between the Cadia region and the evolution of the Lachlan fold belt. It is notable that the high-grade Ridgeway deposit is up to 18 m.y. older than any alkalic porphyry deposit yet discovered in the Macquarie arc, a feature that may be important for continued exploration success in this region.

Introduction

Numerous studies of porphyry and epithermal gold-copper deposits have attempted to determine the absolute age of mineralization, in addition to the age of the intrusive rocks to which ore deposition is thought to be related (e.g., Marsh et al., 1997; Richards et al., 1999; Garwin, 2000; Gustafson et al., 2001; Lund et al., 2002; Harris et al., 2004). In recently formed deposits (Pliocene and younger), precise geochronometers have enabled the absolute longevity of the hydrothermal system that led to ore deposit formation to be determined (e.g., Lepanto-Far Southeast: Arribas et al., 1995; Batu Hijau: Garwin, 2000). Detailed geochronology also has identified the occurrence of multiple, temporally discrete mineralizing events within single mineral districts (e.g., Potrerillos: Marsh et al., 1997; Indio Muerto: Gustafson et al., 2001; Boulder batholith: Lund et al., 2002).

Most of these detailed studies have focused on porphyry-epithermal districts that occur in Tertiary volcanic arcs. This paper discusses the geochronology of porphyry gold-copper deposit formation in the Cadia district of eastern Australia, which formed within a Paleozoic intraoceanic island-arc terrane known as the Macquarie arc (Glen et al., 1998).

New data generated by this study comprise seven U-Pb ages for magmatic zircon and titanite from intrusions spatially and, in some cases, genetically related to the Cadia district porphyry deposits, and five Re-Os ages for molybdenite from three Cadia porphyry deposits. These data have been used to

[†] Corresponding author: e-mail, alanwilson@angloamerican.com.au

[*] Present address: Anglo American Exploration (Australia) Pty Ltd, Suite 1, 16 Brodie-Hall Drive, Bentley, Western Australia 6102, Australia.

provide constraints on the absolute timing of magmatic and hydrothermal activity in the Cadia district. The Paleozoic age of these deposits precludes a determination of the absolute longevity of discrete hydrothermal systems, due to the fact that analytical and decay constant uncertainties in rocks of this age are larger than the duration of typical porphyry systems (cf. Arribas et al., 1995; Watanabe et al., 1999). However, valuable insight into the cyclical nature of ore-related magmatic activity within the district has been gained. This, in turn, impacts geologic models for the tectonic setting of ore deposit formation, our understanding of the geologic evolution of the Macquarie arc, and exploration criteria for similar deposits elsewhere in this region.

Geologic Setting

Regional geology, geochronology, and mineral deposits

The geology of the Cadia region has been described by Holliday et al. (2002) and Wilson et al. (2003) and is summarized briefly here. The Macquarie arc was an intraoceanic island arc that developed off the eastern margin of the Australian plate from the earliest Ordovician to the earliest Silurian (Glen et al., 2003) in a tectonic setting similar to that of the present-day southwest Pacific Ocean. The current geometry of the arc-related rocks, as four separate belts, is attributed to splitting of a single arc by pure extension or sinistral strike-slip faulting (Fig. 1; Scheibner, 1973; Packham,

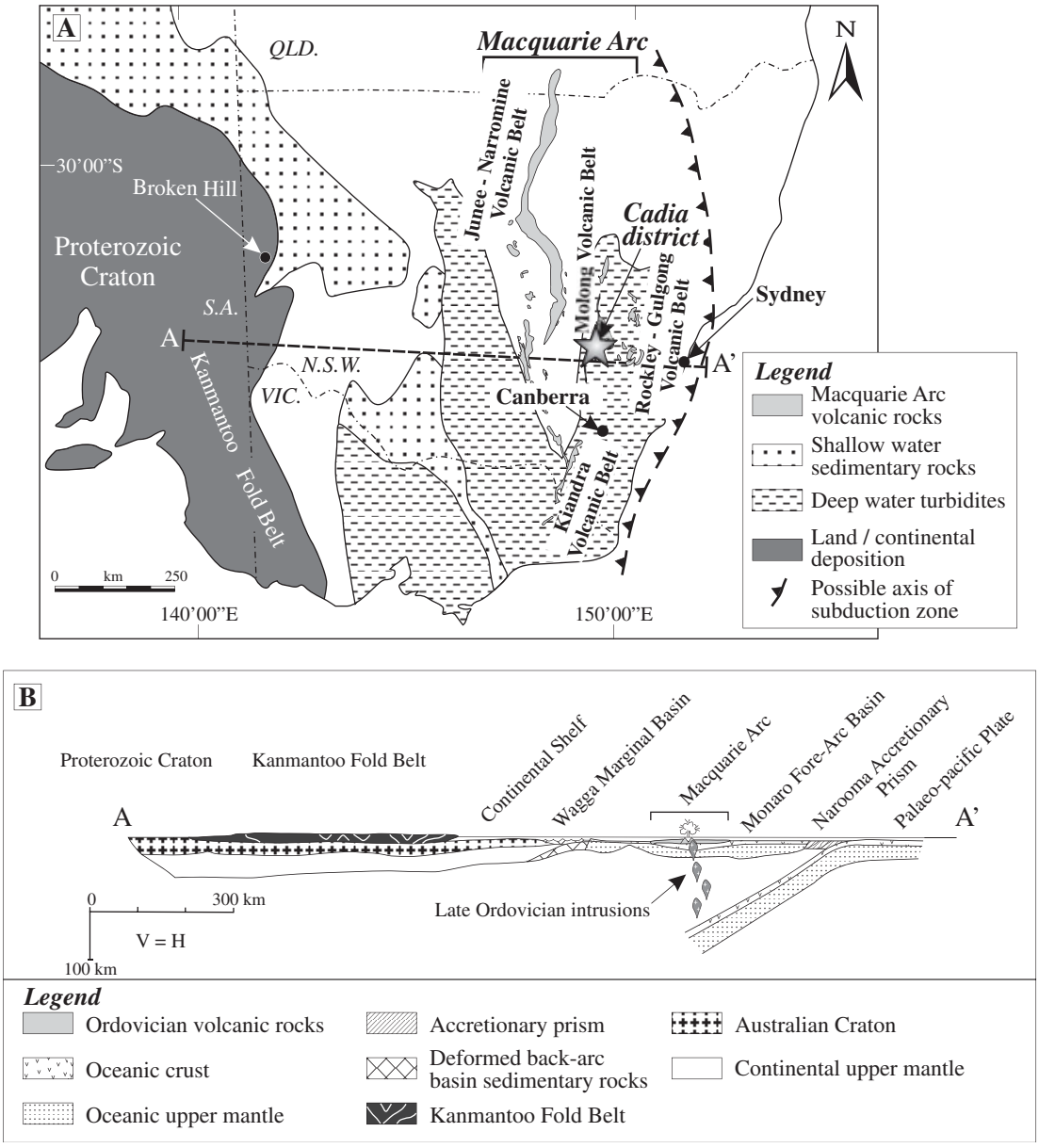

FIG. 1. A. Simplified paleogeographic interpretation of southeastern Australia, showing the Lachlan fold belt during the Late Ordovician. The present-day geometry of Macquarie arc volcanic rocks and location of the Cadia district are also shown. B. Schematic cross section A-A', showing a reconstruction of the geology of the Lachlan fold belt during the Late Ordovician. A west-dipping subduction zone is inferred to have generated the intraoceanic Macquarie arc (Scheibner and Basden, 1998). Modified from Scheibner and Basden (1998) and Scheibner and Veevers (2000).

1987; Glen et al., 1998). The arc is postulated to have developed above a west-dipping subduction zone from the Early to Late Ordovician, with volcanic hiatuses during the Middle Ordovician and Eastonian (A.J. Crawford, pers. commun., 2004; Fig. 1B). Geophysical (seismic-reflection: Glen et al., 2002) and geochemical (ε_{Nd}: Wyborn and Sun, 1993; Pb isotopes: Carr et al., 1995) data indicate that the arc developed on a substrate of oceanic crust, with little evidence for input from continental crust.

Based on evidence from the two larger volcanic belts (the Junee-Narromine and Molong volcanic belts; Fig. 1), Glen et al. (2003) proposed that the Macquarie arc developed episodically over a period of about 50 m.y. Three pulses of volcanic activity in these belts (Early Ordovician, ~490–475 Ma; Middle Ordovician, 464–455 Ma; Late Ordovician to Early Silurian, 450–439 Ma) were separated by two major volcanic hiatuses (~470 ± 5 and 452 ± 2 Ma). Glen et al. (2003) also recognized four groups of porphyritic intrusive rocks in the Macquarie arc: Group 1, ~484 Ma high K calc-alkalic to shoshonitic monzonites; Group 2, 465 to 455 Ma high K calc-alkalic monzogabbros to monzonites; Group 3, 455 to 450 Ma medium K calc-alkalic dacites; Group 4, ~439 Ma shoshonitic monzodiorites to quartz monzonite porphyries.

The Macquarie arc hosts the types of gold and gold-copper deposits that are typical of modern and ancient volcanoplutonic arcs around the world (Holliday et al., 2002; Fig. 2). Alkalic porphyry gold-copper deposits at Cadia (Holliday et al., 2002, Wilson et al., 2003) and Northparkes (Heithersay et al., 1990; Heithersay and Walshe, 1995; Lickfold et al., 2003) occur in association with Late Ordovician to Early Silurian shoshonitic monzonite to quartz monzonite intrusions (Group 4 porphyries of Glen et al., 2003). However, based on the results of this study, a more complex magmatic-hydrothermal history is now proposed for the Cadia district. U-Pb dating of zircon from shoshonitic intrusions of the Goonumbla region

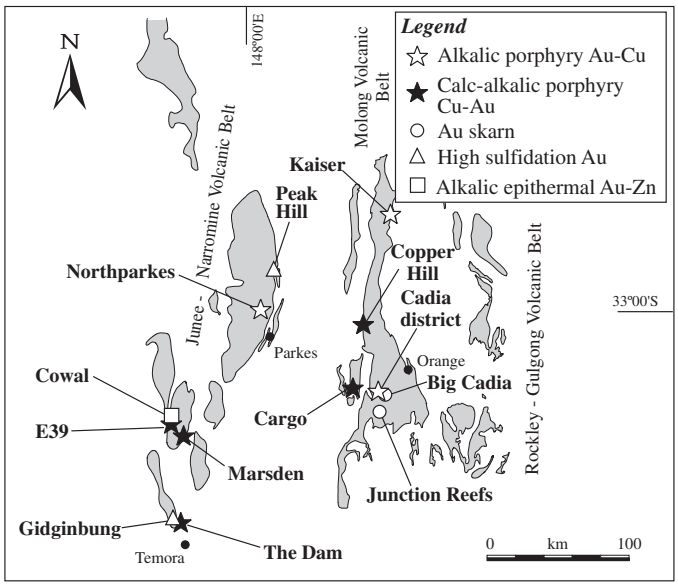

FIG. 2. Location of principal porphyry, skarn, and epithermal deposits of the Macquarie arc. No known mineral deposits occur in the Kiandra volcanic belt, which crops out to the south of the region shown here (Fig. 1). Modified from Holliday et al. (2002).

indicates episodic magmatic activity from 484 to 439 Ma (Butera et al., 2001; Lickfold et al., 2003), although $^{40}Ar/^{39}Ar$ analysis of biotite and hornblende indicate that gold-copper mineralization and related alteration occurred between 446 and 437 Ma, (Lickfold et al., 2003). Calc-alkalic porphyry copper-gold deposits are associated with medium K intrusive dacites at the ~450 Ma Copper Hill deposit (Scott, 1976, 1978) and also at Cargo (Richardson, 1976; Richardson et al., 1983). Similar deposits associated with medium K diorites to quartz monzonites at Marsden and Cowal (e.g., E39; Miles and Brooker, 1998) may belong to the ~439 Ma Group 4 porphyries of Glen et al. (2003). Gold- and copper-rich skarn deposits at Junction Reefs (Gray et al., 1995) and Big Cadia (Green, 1999; Forster et al., 2004) are hosted by Eastonian-aged calcareous sandstones and limestones (~448 Ma: Packham et al., 1999) that occur proximal to shoshonitic monzodiorite to quartz monzonitic stocks. Using $^{40}Ar/^{39}Ar$ and U-Pb geochronology, Perkins et al. (1992) identified the presence of 480 to 470 Ma monzodioritic intrusions in the Junction Reefs area, although skarn mineralization was interpreted to be related to a younger (~439 Ma) magmatic-hydrothermal event. Small and highly deformed high-sulfidation deposits, with a close spatial association to major fault zones, occur at Peak Hill (Degeling et al., 1995; Masterman et al., 2002) and Gidginbung (Thompson et al., 1986), in addition to a calc-alkalic porphyry occurrence at the Dam (Fig. 2). Finally, a structurally controlled gold-zinc deposit of probable carbonate-base metal epithermal affinity (cf. Corbett and Leach, 1998) occurs at Cowal (E42: Bastrakov et al., 1996; Miles and Brooker, 1998; Bywater et al., 2004).

Local geology

The porphyry deposits of the Cadia district are temporally and spatially associated with small, vertically attenuated intrusive complexes of shoshonitic monzodiorite to quartz monzonite composition. They were emplaced within a 6-km-long, west-northwest–oriented corridor (Fig. 3) that lies parallel to the Lachlan transverse zone, an interpreted major precratonic structural feature of eastern and central Australia (Glen and Walshe, 1999). Host rocks of the porphyry-related intrusions comprise a thick sequence (>2 km) of fine- to coarse-grained, mafic to intermediate volcanogenic sedimentary rocks of the Middle Ordovician Weemalla Formation and overlying Late Ordovician Forest Reefs Volcanics (Fig. 3; Pogson and Watkins, 1998). A major structural feature of the district is the roughly north-striking Cadiangullong fault zone. The Forest Reefs Volcanics to the west of this fault zone contain predominantly andesitic volcanic clasts, whereas clasts in the Forest Reefs Volcanics east of the fault zone are mainly of basaltic composition, suggesting two different source regions for the Forest Reefs Volcanics (Wilson, 2003). Limestone and calcareous sandstone units occur locally within the upper portion of the Forest Reefs Volcanics. Based on conodont assemblages in the calcareous units, these rocks are interpreted to be of late Eastonian age (middle Late Ordovician: Packham et al., 1999; Fig. 3). Interpretation of lithofacies of the Weemalla Formation and Forest Reefs Volcanics suggests that the Cadia district underwent a transition from a position distal to a volcanic center during the Middle Ordovician to one proximal to an

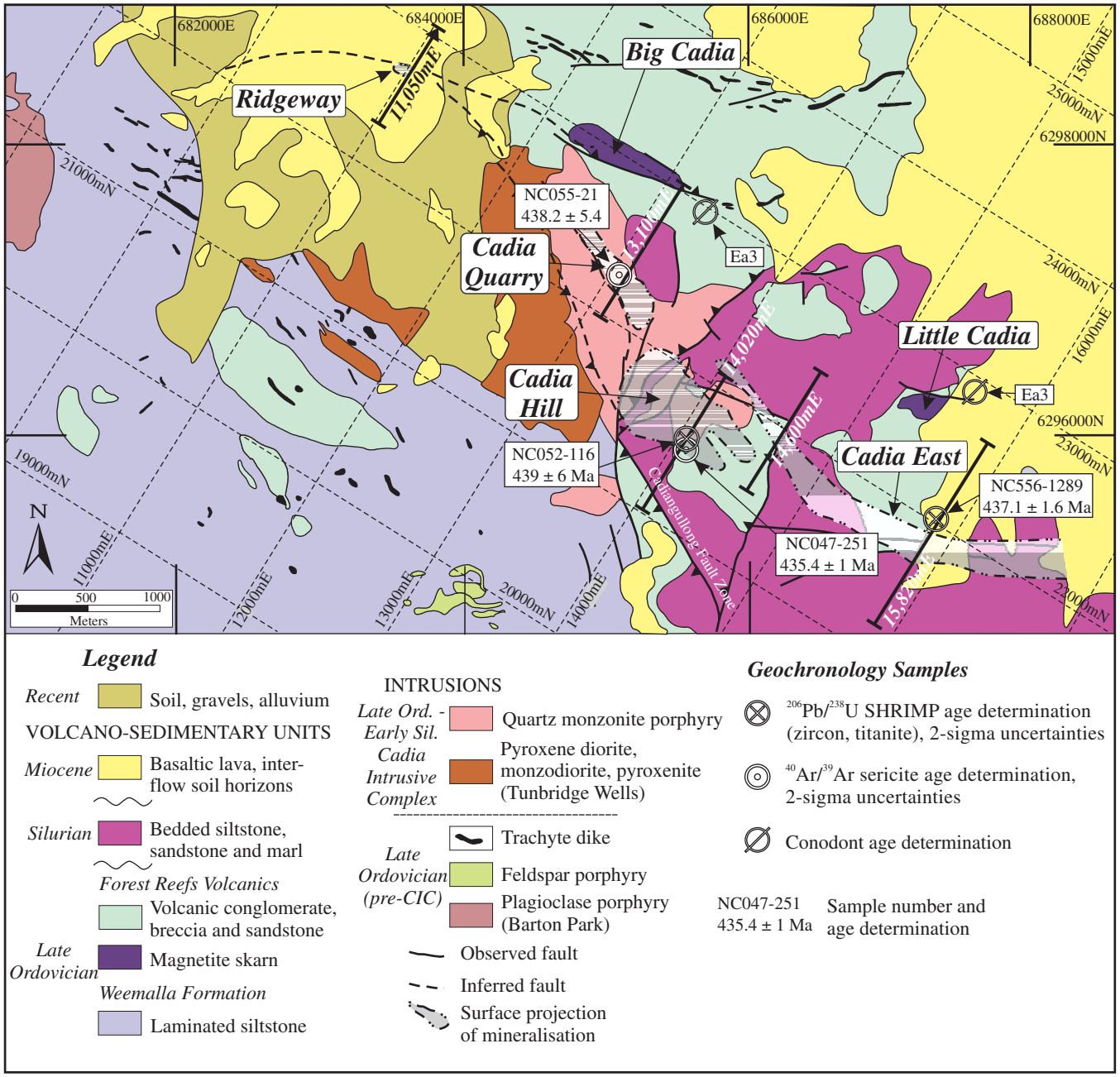

FIG. 3. Summary geology map of the Cadia district, showing previous age determinations. SHRIMP ages from L. Black (1994, unpub. report for Newcrest Mining Ltd.) and Squire (2001), and sericite ages from C. Perkins (1994, unpub. report for Newcrest Mining Ltd.) and Forster et al. (2004). Conodont ages from Packham et al. (1999). Geologic map modified from Holliday et al. (2002). CIC = Cadia Intrusive Complex, Ord. = Ordovician, Sil. = Silurian.

emergent volcano during the Late Ordovician to earliest Silurian (Squire, 2001; Wilson, 2003).

Ore-related intrusions range in composition from pyroxene-phyric monzonite to quartz monzonite, whereas premineral, comagmatic intrusions are gabbroic to monzodioritic. Holliday et al. (2002) reported that the main body of quartz monzonite at Cadia Hill is compositionally and petrographically identical to unexposed monzodiorite to quartz monzonite intrusions at Ridgeway and Cadia East. All of the intrusions are shoshonitic (Holliday et al., 2002), and a high oxidation state for these magmas is indicated by high modal abundance of magnetite, Mg-rich biotite, and high whole-rock Fe_2O_3/FeO ratios (Blevin, 2002). A mature oceanic-arc setting is indicated on the tectonic discrimination diagrams of Müller et al. (1992). Values of $^{87}Sr/^{86}Sr$ (0.7042–0.7045) and ε_{Nd} (5.0–5.4) for these monzonitic intrusions preclude the interaction of these igneous rocks with continental crustal material (Wilson, 2003).

Local extension along regional-scale, deep-seated structures within the Lachlan transverse zone during the Late

Ordovician to Early Silurian is interpreted to have facilitated the tapping of a subduction-modified depleted mantle source and genesis of the highly oxidized shoshonitic magmas (Wilson, 2003). The present-day west to northwest strike of the monzonitic intrusive complexes is interpreted to suggest emplacement of intrusions within locally developed zones of north- to northeast-oriented extension that formed in response to regional-scale west-northwest-oriented dextral strike-slip faulting (Wilson, 2003). However, the local distribution of high-grade gold-copper mineralization at Cadia East suggests a sinistral sense of movement along west-northwest–oriented faults at the time of ore deposition in this deposit (I. Tedder, pers. commun., 2004).

Uplift and erosion of the Cadia district during the Early Silurian exposed the Cadia Quarry, Cadia Hill, and Cadia East deposits prior to the deposition of Middle to Late Silurian shale and fossiliferous sandstone (Fig. 3). Evidence for unroofing of the deposits is provided by clasts of monzonite and magnetite skarn in the basal Silurian conglomerate. Unconformable Miocene basalts of the Canobolas Volcanic Complex (Wellman and McDougall, 1974) locally overlie Ordovician and Silurian rocks of the Cadia district.

Porphyry Deposits of the Cadia District

Two styles of porphyry deposit have been defined within the Cadia district: "intrusion-related" deposits and "intrusion-hosted" deposits (Wilson et al., 2002; Wilson, 2003). Intrusion-related deposits are those in which mineralization is localized within and around a temporally and genetically related intrusive complex (e.g., Ridgeway: Wilson et al., 2003; Cadia East: Wilson, 2003). In contrast, intrusion-hosted deposits are those in which mineralization is hosted within monzonite, but there is no textural evidence to support a direct genetic link between mineralization and the host intrusion (e.g., Cadia Quarry: Wilson et al., 2004; Cadia Hill: Wilson, 2003).

Alteration assemblages at the four porphyry deposits have been grouped into early, transitional, and late stages (Wilson et al., 2003, 2004). Early-stage alteration is characterized by magnetite-bearing sodic (albite), sodic-calcic (albite-actinolite), potassic (biotite-orthoclase), and calc-potassic (actinolite-biotite-magnetite-orthoclase) assemblages. Transitional-stage potassic alteration (orthoclase-biotite) typically occurs as envelopes around mineralized quartz-calcite veins, and propylitic alteration (chlorite-actinolite-epidote-calcite-hematite) occurs peripheral to the potassic alteration zones. Ore is associated with both early- and transitional-stage alteration assemblages. Late-stage alteration is characterized by locally developed pervasive feldspar (orthoclase-albite) alteration and structurally focused phyllic (illite-muscovite-pyrite-calcite-quartz) assemblages.

Previous Geochronological Studies

Prior to the current study, several attempts have been made to date the magmatic and hydrothermal activity at Cadia. Ambler et al. (1977) reported an Rb-Sr whole-rock age of 423 ± 8 Ma for monzonitic rocks of the Cadia Intrusive Complex in the Cadia Quarry area, although the precise location of the sample site cannot be established. This age contrasts with a $^{206}Pb/^{238}U$ SHRIMP zircon age of 439.0 ± 6 Ma for a quartz monzonite porphyry at Cadia Hill (L. Black, 1994, unpub. report for Newcrest Mining Ltd.) and a $^{206}Pb/^{238}U$ SHRIMP zircon age of 437.1 ± 1.6 Ma for an intermineral quartz monzonite porphyry dike from the Cadia East deposit (Squire, 2001; Fig. 3). The SHRIMP data are interpreted to suggest that the intrusive rocks spatially associated with mineralization at Cadia Hill and Cadia East were emplaced around 438 Ma (Early Silurian according to the timescale of Cooper, 1999, corresponding to the age of the Group 4 porphyries of Glen et al., 2003). The Middle Silurian Rb-Sr age of Ambler et al. (1977) is considered to reflect the lack of closed-system behavior of the Rb-Sr system, perhaps due to thermal overprinting of the intrusions subsequent to their emplacement.

Two $^{40}Ar/^{39}Ar$ ages for hydrothermal white mica from Cadia Hill have been determined, although neither sample yielded a true plateau (C. Perkins, 1994, unpub. report for Newcrest Mining Ltd.; Fig. 3). The best interpretation of these samples is that alteration and mineralization occurred between 439 and 435 Ma and that a younger age of 425 Ma represents the timing of white mica recrystallization in response to open system behavior (C. Perkins, 1994, unpub. report for Newcrest Mining Ltd.). Additionally, Forster et al. (2004) recorded a $^{40}Ar/^{39}Ar$ age of 438.2 ± 5.4 Ma (2σ uncertainty) for muscovite associated with quartz sulfide veins at Cadia Quarry (Fig. 3), consistent with previous $^{40}Ar/^{39}Ar$ and U-Pb ages.

U-Pb SHRIMP Analytical Method

U-Pb age determinations for magmatic zircon and titanite were obtained using the Sensitive High Resolution Ion Micro-Probe (SHRIMP) at the Research School of Earth Sciences, Australian National University. Heavy mineral concentrates were prepared using standard crushing, desliming, heavy liquid, and paramagnetic techniques. Where present, the zircons were handpicked from the mineral concentrates, mounted in epoxy together with chips of the FC1 Duluth Gabbro reference zircon (Paces and Miller, 1993), sectioned approximately in half, and polished. Reflected and transmitted light photomicrographs and cathodoluminescence (CL) scanning electron microscope images were prepared for all zircons to determine the internal structures of sectioned grains and so target areas within zoned magmatic zircon. When no zircons were found, magmatic titanite was handpicked and mounted together with a reference titanite from the Khan pegmatite (518 Ma; R. Armstrong, pers. commun., 2004). The titanite probe mount was prepared and photographed as described above, except that backscattered secondary electron (BSE) images were taken of each of the sectioned titanite grains.

U-Pb analyses for zircon and titanite were performed using SHRIMP II (sample NC083-035 using SHRIMP I; SHRIMP suffix reflects machine used to conduct analyses), each analysis consisting of six scans through the mass range. The data have been reduced in the manner described by Williams (1998) and references therein, using the SQUID Excel macro of Ludwig (2001). For zircon, the Pb/U ratios have been normalized relative to a value of 0.1859 for the $^{206}Pb/^{238}U$ ratio of the FC1 reference zircons, equivalent to an age of 1099 Ma (Paces and Miller, 1993). The Pb/U ratio data from titanite have been normalized relative to a value of 0.08367 for the $^{206}Pb/^{238}U$ ratio of the Khan reference titanite, equivalent to an age of 518 Ma. Corrections for common lead were made using the measured $^{206}Pb/^{238}U$ and

$^{206}Pb/^{207}Pb$ ratios, following Tera and Wasserburg (1972), as outlined in Compston et al. (1992). These are minimal as the majority of the zircon areas analyzed are low in common Pb; the analyses plot close to, or within analytical uncertainty of the Tera-Wasserburg Concordia curve (not shown). Uncertainties given for individual analyses (ratios and ages) are at the 1σ level; however, all uncertainties in calculated weighted mean ages are reported as 95 percent confidence limits. Relative probability plots, with stacked histograms of the radiogenic $^{206}Pb/^{238}U$ ages and ensuing weighted mean calculations were made using Isoplot/Ex (Ludwig, 2003).

U-Pb SHRIMP Results

Seven new $^{206}Pb/^{238}U$ SHRIMP age determinations for magmatic zircon and titanite have been obtained from the four porphyry deposits of the Cadia district (Table 1, App.). The intrusive rock samples were selected from different igneous complexes in the Cadia district to determine age relationships between and within the intrusive complexes. The spatial relationship between these samples is shown in an interpreted geologic long section of the Cadia district (Fig. 4).

Ridgeway

Based on crosscutting relationships between veins and intrusions, the Ridgeway Intrusive Complex and the Ridgeway orebody are interpreted to have formed contemporaneously (Wilson et al., 2003). This study focuses on determining the age of the premineral mafic monzonite and the intermineral quartz monzonite porphyry in order to relate intrusive activity to the timing of mineralization. No molybdenite was found at Ridgeway that would have enabled direct dating of the mineralization.

Magmatic titanite from the pyroxene-phyric monzonite phase of the Ridgeway Intrusive Complex (sample NC498-569) has a weighted average $^{206}Pb/^{238}U$ age of 456.9 ± 7.2 Ma (MSWD = 1.14), and zircon from the intermineral quartz monzonite porphyry (sample NC498-809) has a weighted average $^{206}Pb/^{238}U$ age of 455.8 ± 4.4 Ma (MSWD = 1.30; Table 1, Figs. 4, 5A). The titanite age determinations cluster as a single population on a relative probability plot (Fig. 5B) and backscattered electron images of titanite crystals show that they either lack internal structure or show simple continuous magmatic zonation from center to edge (Fig. 5C). The zircon analyses from the intermineral quartz monzonite porphyry also form a single population on the relative probability plot (Fig. 5D), indicating that zircon inheritance or lead loss has not affected the interpretation of the age of this sample. From these data, the Ridgeway Intrusive Complex and, by inference, the Ridgeway mineralization formed at about 456 ± 6 Ma (mean of $^{206}Pb/^{238}U$ ages determined by this study).

Cadia Quarry

The Cadia Quarry orebody comprises an envelope of sheeted quartz veins that transect a large and texturally variable intrusive complex of quartz monzonite to quartz monzodiorite porphyry (Fig. 3; Wilson et al., 2004). Three $^{206}Pb/^{238}U$ ages of intrusions that host mineralization and those to the southwest of the orebody have been determined (Table 1, Figs. 4, 6).

Two quartz monzonite porphyry samples from outside of the main orebody have interpreted magmatic zircon crystallization $^{206}Pb/^{238}U$ weighted average ages of 456.4 ± 5.1 Ma (sample NC083-035; MSWD = 1.20; Fig. 6A-B) and 453.4 ± 4.3 Ma (sample NC486-467; MSWD = 0.41; Fig. 6D). Both of these samples also contain a younger population of zircon (429.7 ± 4.2 and 438.7 ± 5.1 Ma, respectively; Fig. 6B, D) that can be interpreted to reflect either radiogenic Pb loss or a second period of zircon growth. Evidence for radiogenic Pb

TABLE 1. New SHRIMP $^{206}Pb/^{238}U$ Age Determinations in the Cadia District

Sample[1]	Description	Intrusive complex	Interpreted age [2]	Age[3] (Ma)	2σ[4] (Ma)	MSWD	No. spots
Ridgeway							
NC498-569	Equigranular clinopyroxene-hornblende mafic monzonite	RIC	Magmatic	456.9	±7.2	1.14	13
NC498-809	Clinopyroxene-hornblende quartz monzodiorite porphyry	RIC	Magmatic	455.8	±4.4	1.30	19
Cadia Quarry							
NC083-035	Clinopyroxene-biotite quartz monzonite porphyry	Western CIC	Magmatic	456.4	±5.1	1.20	10
			Pb loss	429.7	±4.2	1.05	10
NC486-467	Hornblende-biotite quartz monzodiorite porphyry	Western CIC	Magmatic	453.4	±4.3	0.41	12
			Pb loss	438.7	±5.1	0.13	7
NC486-608	Clinopyroxene-hornblende quartz monzodiorite porphyry	Eastern CIC	Magmatic	436.5	±3.5	1.05	19
Cadia Hill							
NC384-200	Clinopyroxene-hornblende quartz monzodiorite porphyry	Eastern CIC	Magmatic	435.9	±3.7	0.78	16
Cadia East							
NC475-1247	Clinopyroxene-hornblende quartz monzodiorite porphyry	CFEIC	Magmatic	451.0	±1.4	1.20	14

Abbreviations: CFEIC = Cadia Far East Intrusive Complex, CIC = Cadia Intrusive Complex, RIC = Ridgeway Intrusive Complex

[1] The number before the hyphen is the drill hole from which the sample was collected; the number after the hyphen is the depth in meters from which the sample was collected

[2] Magmatic and Pb loss ages are interpreted from the integrated SHRIMP data and textural features of the grains analyzed; see text for discussion

[3] Weighted average ages were calculated using Isoplot (Ludwig, 2003); all analyses were conducted at the Australian National University

[4] All uncertainties are at 95% confidence levels

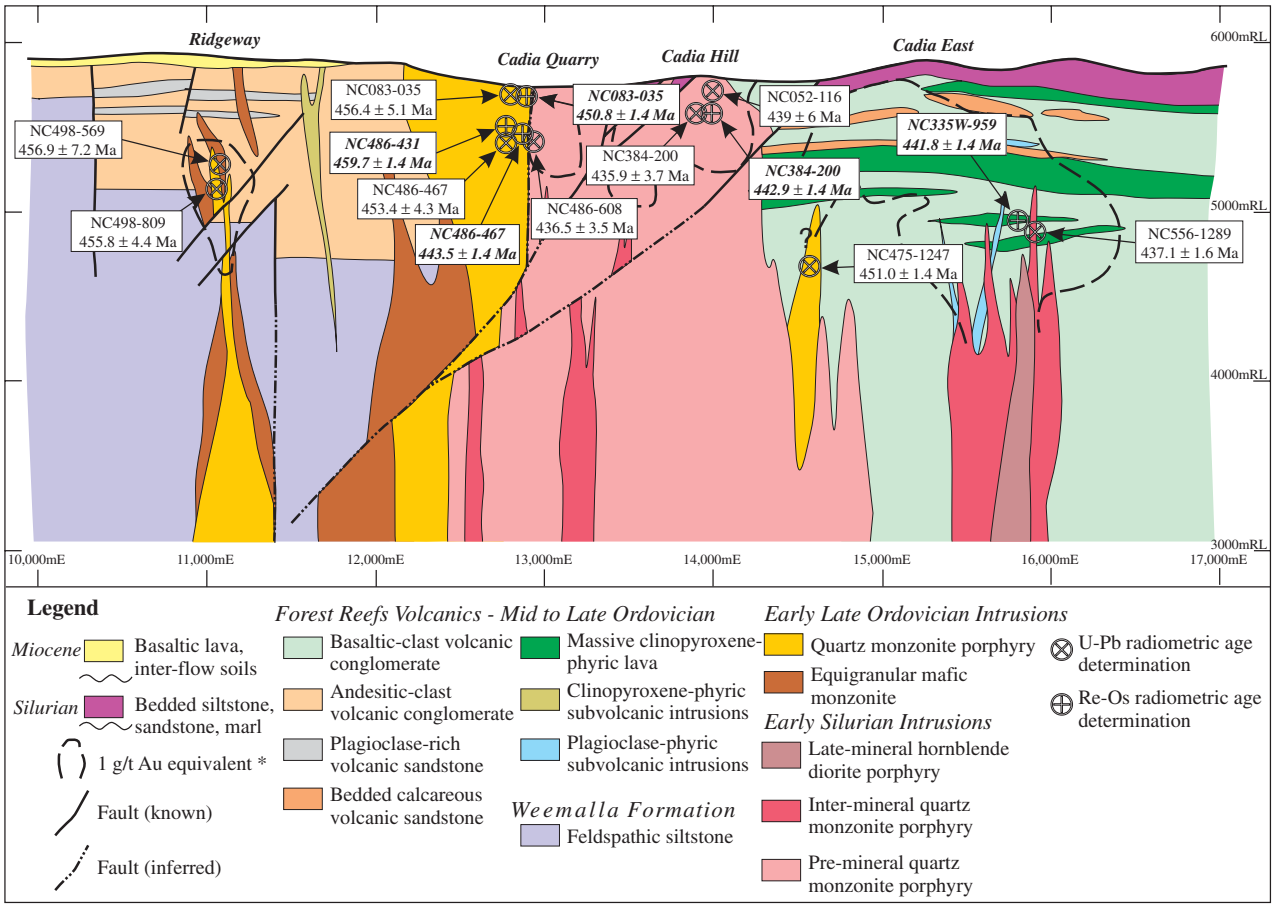

FIG. 4. Interpreted long section of the Cadia district (modified from Tedder et al., 2001), showing U-Pb and Re-Os ages. Also shown is the 1.0 g/t Au equivalent grade contours for each of the deposits. Gold equivalent was calculated using the formula 1.8 percent Cu = 1g/t Au.

loss includes serrated and ragged morphology of the younger grains in sample NC083-035 (Fig. 6C). CL imagery of the grains revealed complex patterns of magmatic zonation, with evidence of zoned core and rim components (Fig. 6C, E). However, analyses of these components revealed no consistent relationship between age and location within the zircon grain, adding further support to the radiogenic Pb loss hypothesis for the younger age populations.

The third quartz monzonite porphyry sample (NC486-608) was taken from the center of the Cadia Quarry orebody and yielded a $^{206}Pb/^{238}U$ weighted average age of 436.5 ± 3.5 Ma (MSWD = 1.05; Fig. 6F) based on a single zircon population. Although CL imagery of these zircons revealed them to be internally complex, with zoned core and zoned rim components (Fig. 6G), SHRIMP analyses of cores and rims indicated the presence of a single age population, with no evidence for radiogenic Pb loss.

Cadia Hill

Zircon from one sample of quartz monzonite porphyry from the Cadia Intrusive Complex at Cadia Hill returned a $^{206}Pb/^{238}U$ weighted average age of 435.9 ± 3.7 Ma (MSWD = 0.78; Table 1, Figs. 4, 7), based on a single zircon population (Fig. 7B). Two analyses that returned an age of ~ 451 Ma were excluded from the calculation of the weighted average age and may be inherited grains. Two grains with relatively high contents of common lead were also excluded. However, the relative probability plot of all zircon areas analyzed from this sample defines a simple bell-shaped curve, representing a single age population. Inclusion of these grains in the weighted average calculation does not significantly change the age of the sample (436.7 ± 4.5 Ma, MSWD = 1.12).

Cadia East

Zircon from a weakly mineralized quartz monzodiorite porphyry dike (NC475-1247) from the western end of Cadia East returned a weighted average $^{206}Pb/^{238}U$ age of 451.0 ± 1.4 Ma (MSWD =1.20; Table 1, Fig. 8). In a relative probability plot, these analyses plot as a bimodal population, with dispersion on the younger side of the peak at 440.1 ± 4.2 Ma that may represent minor radiogenic Pb loss or a second period of zircon growth (Fig. 8B).

Re-Os Analytical Method

Total Re and ^{187}Os concentrations of eight aliquots of molybdenite from five samples of quartz vein-hosted molybdenite were determined at AIRIE, Colorado State University. A Carius-tube digestion was used (Shirey and Walker, 1995), whereby molybdenite was dissolved and equilibrated with single ^{185}Re and ^{190}Os spikes in HNO_3-HCl (inverse aqua regia)

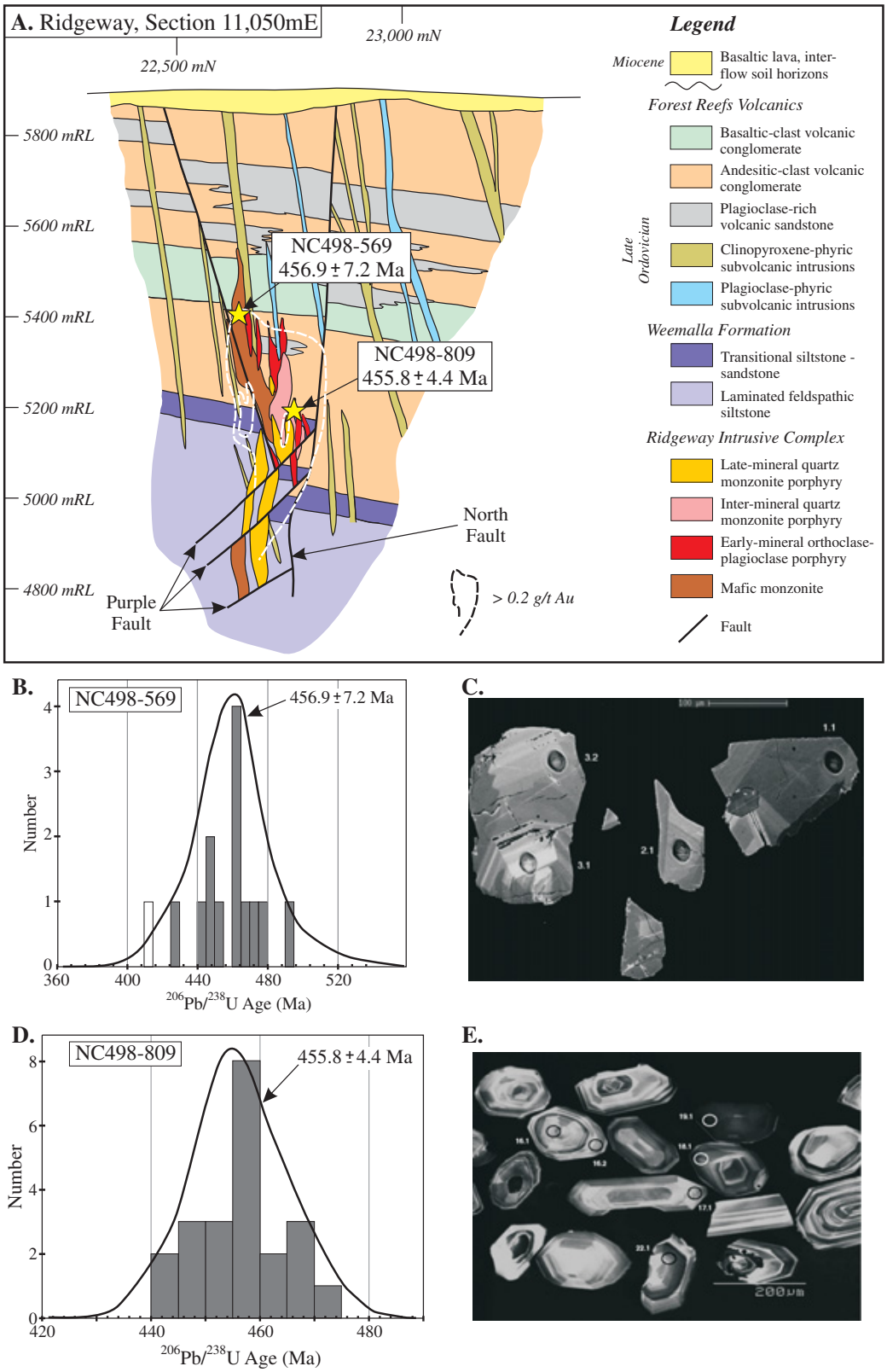

FIG. 5. U-Pb age determinations from Ridgeway. A. Location and SHRIMP ages in section 11,050 mE. See Figure 3 for section location. B. Relative probability plot of titanite SHRIMP analyses, sample NC498-569. The analysis represented by the white bar is considered to reflect radiogenic Pb loss and has not been included in weighted average age calculation. C. Backscattered electron image of titanite from sample NC498-569. D. Relative probability plot of zircon SHRIMP analyses, sample NC498-809. E. Cathodoluminescence image of zircon from sample NC498-809. Numbers in images in (C) and (E) mark the location of SHRIMP analyses as detailed in the Appendix.

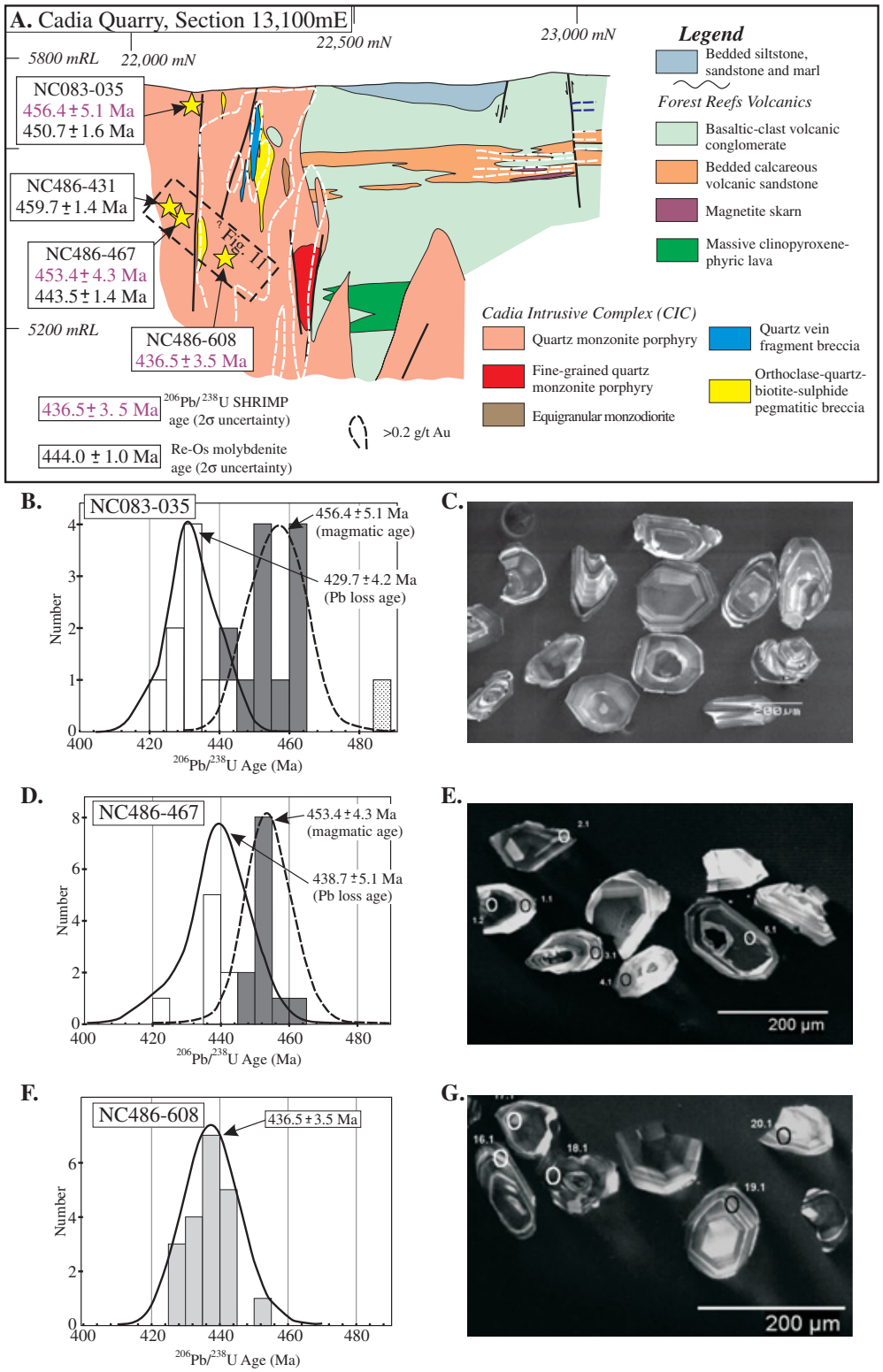

FIG. 6. U-Pb and Re-Os age determinations from Cadia Quarry. A. Location and ages in section 13,100 mE. See Figure 3 for section location. B. Relative probability plot of zircon SHRIMP analyses, sample NC083-035. C. Cathodoluminescence (CL) image of zircon from sample NC083-035. D. Relative probability plot of zircon SHRIMP analyses, sample NC486-467. E. CL image of zircon from sample NC486-467. F. Relative probability plot of zircon SHRIMP analyses, sample NC486-608. G. CL image of zircon from sample NC486-608. Dark- and light-gray filled bars in probability plots represent interpreted magmatic age for older and younger intrusions, respectively. White bars are analyses considered to have lost radiogenic Pb. The stippled bar represents an older analysis (inherited grain?) that has not been included in weighted average age calculations. Numbers in images in (C), (E), and (G) mark the location of SHRIMP analyses as detailed in the Appendix.

by sealing in a thick-walled glass ampoule and heating for 12 h at 230°C. The Os was recovered by distilling directly from the Carius tube into HBr and was subsequently purified by microdistillation. The Re was recovered by anion exchange. The Re and Os were loaded onto Pt filaments and isotopic compositions are determined using NTIMS on NBS 12-in radius, 68° and 90° sector mass spectrometers at AIRIE. Two in-house molybdenite standards, calibrated at AIRIE, are run routinely as an internal check (Stein et al., 1997; Markey et al., 1998). The age was calculated by applying the equation $^{187}Os = {}^{187}Re(e^{\lambda t} - 1)$, where λ is the decay constant for ^{187}Re and t is the calculated age. The ^{187}Re decay constant used is 1.666×10^{-11}

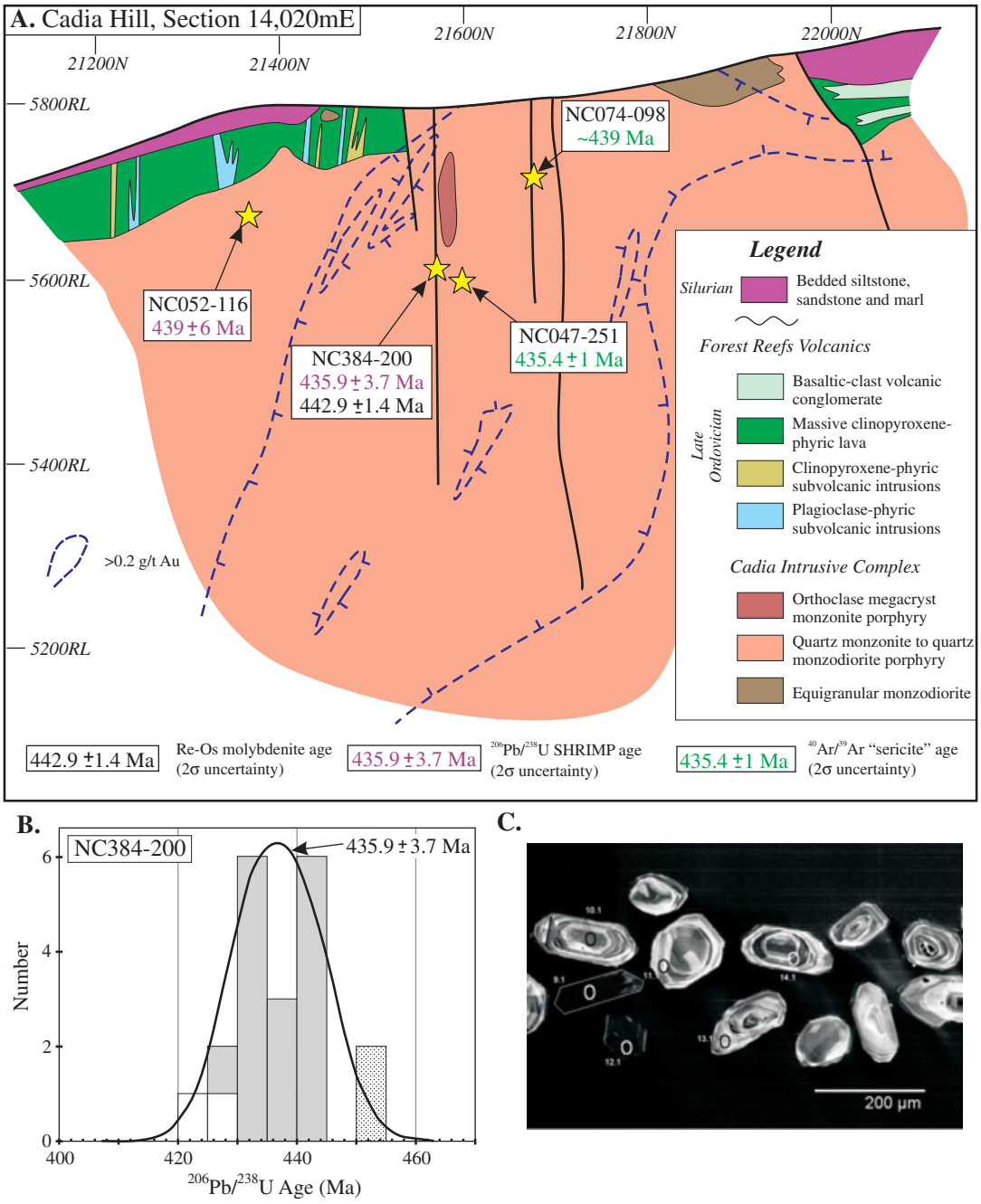

FIG. 7. U-Pb and Re-Os age determinations at Cadia Hill. A. Location and ages in section 14,020 mE. Section location is shown in Figure 3. Note that sample NC384-200 has been projected onto this section from section 13,760 mE, whereas sample NC052-116 lies in the plane of this section. B. Relative probability plot of zircon SHRIMP analyses, sample NC384-200. Two older zircon grains (stippled bar) have not been included in the weighted average age calculation and may be inherited grains, and two younger grains (white bars) with relatively high common lead contents have also been excluded from the weighted average age calculation. C. Cathodoluminescence image of zircon from sample NC384-200. $^{40}Ar/^{39}Ar$ ages from C. Perkins (1994, unpub. report for Newcrest Mining Ltd.). Numbers in image in (C) mark the location of SHRIMP analyses as detailed in the Appendix.

yr^{-1}, with an uncertainty of 0.31 percent (Smoliar et al., 1996). Reported 2σ errors include the propagration of all analytical uncertainties, including the uncertainty in the ^{187}Re decay constant. During the period the samples were analyzed using the single Os spike method (CT series, year 2001), blanks were <20 pg for Re and <3 pg for ^{187}Os. Molybdenite data were blank corrected, although molybdenite rarely requires a blank correction.

More recently, two additional molybdenite samples were analyzed using the new double Os spike method (MDID series, Markey et al., 2003). These results are in good agreement with the single Os spike data (Table 2). Blanks during

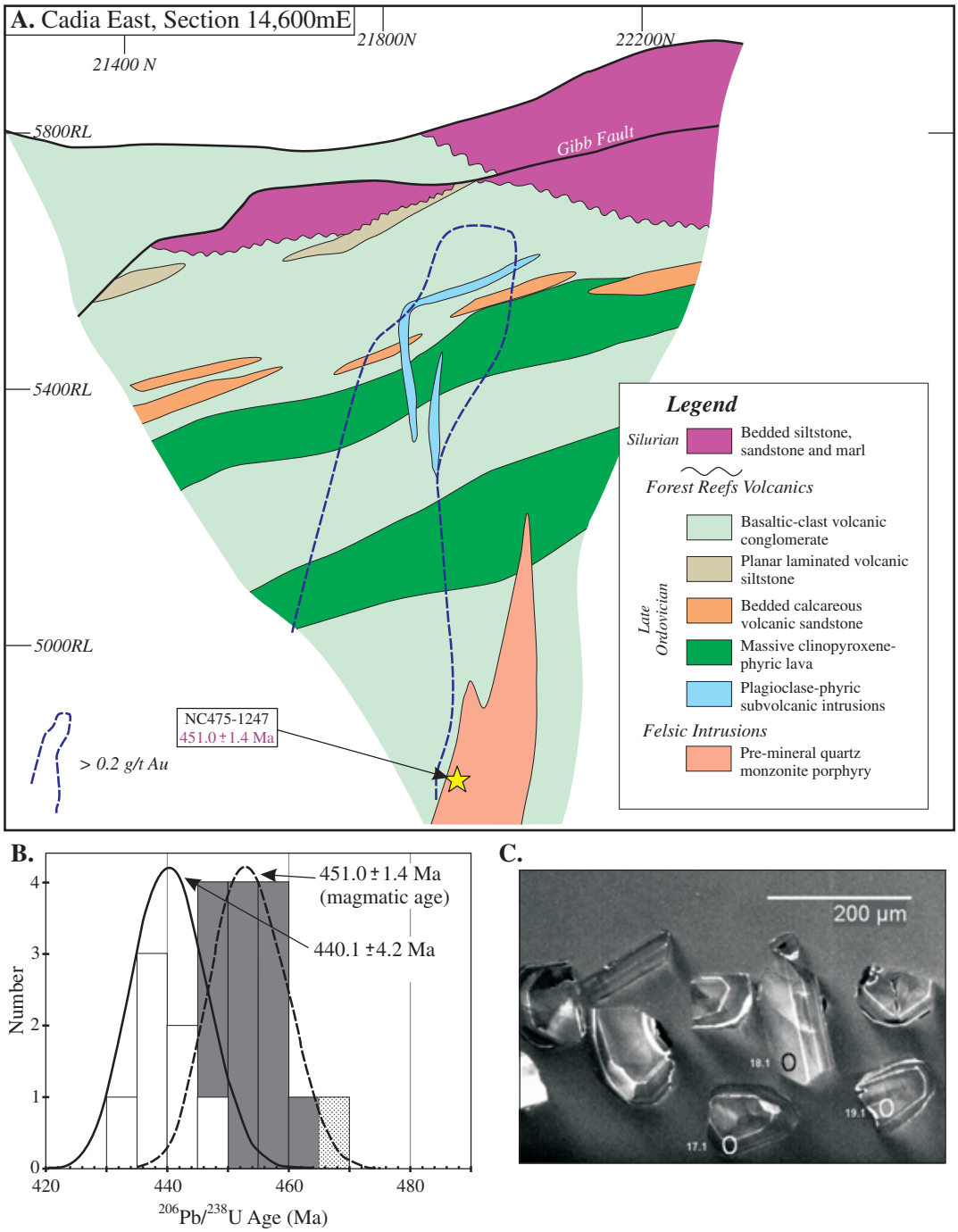

FIG. 8. U-Pb age determinations at Cadia East, section 14,600 mE. A. Interpreted geologic cross section and sample location. B. Relative probability plot of zircon SHRIMP analyses for sample NC475-1247. The older population (dark-gray filled bars) is interpreted as the age for magmatic zircon crystallization, whereas the younger population (white filled bars) is interpreted as the time of radiogenic Pb loss. A single, older analysis (stippled bar) has not been included in the weighted average age calculation and may be an inherited grain. C. Cathodoluminescence image of zircon from sample NC475-1247. Numbers in image in (C) mark the location of SHRIMP analyses as detailed in the Appendix.

TABLE 2. Re-Os Data for Molybdenite from Cadia Porphyry Deposit Transitional-Stage Veins

Sample[1]	Vein description	AIRIE run no.	Re[2] (ppm)	^{187}Os[2] (ppb)	Age[3] (Ma)	Comment[4]
Cadia Quarry						
NC083-035	Stage CH-4A quartz-chalcopyrite-orthoclase-molybdenite vein, orthoclase alteration envelope	CT-306	25.44 (6)	120.4 (1)	450.5 ± 1.7	
		CT-312	25.07 (2)	123.0 (1)	466.6 ± 1.5	Replicate
		CT-335	12.108 (9)	57.37 (3)	450.8 ± 1.4	Replicate
NC486-431	Stage CH-4A quartz-chalcopyrite-molybdenite-calcite vein, no obvious alteration envelope	MDID-195	12.708 (3)	61.40 (3)	459.7 ± 1.4	
NC486-467	Stage CH-4A quartz-molybdenite-chalcopyrite ± calcite vein, orthoclase alteration envelope	CT-406	861 (1)	4013 (5)	443.5 ± 1.4	
Cadia Hill						
NC384-200	Stage CH-4A quartz-chlorite-molybdenite vein, orthoclase alteration envelope	CT-307	203.5 (2)	947 (1)	442.9 ± 1.4	
		MDID-196	170.5 (2)	793.6 (4)	443.0 ± 1.5	Replicate
Cadia East						
NC335W-959	Stage CE-4 quartz-calcite-molybdenite-bornite vein, orthoclase alteration envelope	CT-305	1057 (1)	4909 (5)	441.8 ± 1.4	

[1] The number before the hyphen is the drill hole from which the sample was collected; the number after the hyphen is the drill hole depth in meters

[2] Absolute uncertainties (in parentheses) are shown at the 2σ level for the last digit indicated

[3] Ages were calculated using $^{187}Os = {}^{187}Re\ (e^{\lambda t} - 1)$ and include all analytical and ^{187}Re decay constant uncertainties; decay constant used for ^{187}Re is $1.666 \times 10^{-11}\ yr^{-1}$ (Smoliar et al., 1996)

[4] Molybdenite grain size was generally fine and sample size ranged from 5 to 20 mg; mineral separations were carried out so that entire grains were extracted and thus Re-Os decoupling was not an issue (Stein et al., 2003; Stein, 2006)

these analyses (year 2003) were Re = 1.16 ± 0.3 pg, Os = 1.9 ± 0.1 pg, and $^{187}Os/^{188}Os = 0.25 \pm 0.01$.

Re-Os Results

Eight Re-Os ages of five samples of quartz vein-hosted molybdenite in the Cadia district were determined (Table 2, Fig. 4). Five age determinations were obtained from three transitional-stage quartz veins at Cadia Quarry. Two ages were obtained from two different molybdenite separates taken from a single transitional-stage vein at Cadia Hill. Molybdenite from a transitional-stage vein at Cadia East also was dated. Molybdenite is not present at Ridgeway, and the absolute age of sulfide mineralization remains undetermined in this deposit.

Cadia Quarry

All molybdenite samples originated from transitional-stage quartz sulfide veins that occur peripheral to the Cadia Quarry orebody and are hosted by the older Cadia Quarry quartz monzonite porphyry (Table 2, Figs. 4, 6A; Wilson et al., 2004).

Analysis of a single aliquot of molybdenite from sample NC486-467 returned an Re-Os age of 443.5 ± 1.4 Ma (Fig. 6A), and an older molybdenite age of 459.7 ± 1.4 Ma was determined for a texturally and compositionally similar vein nearby (NC486-431; Fig. 6A). Three separate aliquots of molybdenite from sample NC083-035 returned Re-Os ages of 450.5 ± 1.7, 466.6 ± 1.5, and 450.8 ± 1.4 Ma (Table 2).

These veins are hosted by a quartz monzonite porphyry intrusion that has a U-Pb age of approximately 456-453 ± 5 Ma. The 466.6 Ma molydenite age is older than any rock unit thus far known within the Cadia district and could be a statistical outlier. However, we consider all of the ages in our interpretation, because there was no known analytical problem identified during the analyses.

Cadia Hill

The Cadia Hill quartz monzonite (sample NC384-200; $^{206}Pb/^{238}U$ age of 435.9 ± 3.7 Ma) contains a transitional-stage molybdenite-bearing quartz vein. Analysis of two separate aliquots of molybdenite from this vein returned Re-Os ages of 442.9 ± 1.4 and 443.0 ± 1.5 Ma (Table 2, Figs. 4, 7A). The age of zircon from the immediately adjacent quartz monzonite host rock is slightly younger (this study) than our Cadia Hill molybdenite result, but the 439 ± 6 Ma U-Pb age of the Cadia Hill quartz monzonite porphyry of L. Black (1994, unpub. report for Newcrest Mining Ltd.) overlaps the Re-Os molybdenite ages.

Cadia East

At Cadia East, the Re-Os age of a single aliquot of molybdenite from a transitional-stage quartz sulfide vein is 441.8 ± 1.4 Ma (Table 2, Figs. 4, 9). This vein is hosted by polymict volcanic conglomerates of the Forest Reefs Volcanics but occurs close to an intermineral quartz monzonite porphyry dike that has a $^{206}Pb/^{238}U$ age of 437.1 ± 1.6 Ma (Squire, 2001; Fig. 9).

Geochronology of the Cadia District

Intrusive activity

The results of these new age determinations indicate that the porphyry gold-copper deposits of the Cadia district are the product of at least two temporally discrete intrusive events: Late Ordovician (~456 Ma) and latest Late Ordovician to earliest Silurian (~438 Ma; Fig. 10). The older age is significant because previous $^{40}Ar/^{39}Ar$ and limited SHRIMP U-Pb age determinations for the Cadia porphyry deposits, and for some other alkalic porphyry deposits in the Macquarie arc, have suggested that these deposits were related to a widespread ~446 to 437 Ma (Late Ordovician to Early Silurian) period of shoshonitic magmatism (Perkins et al.,

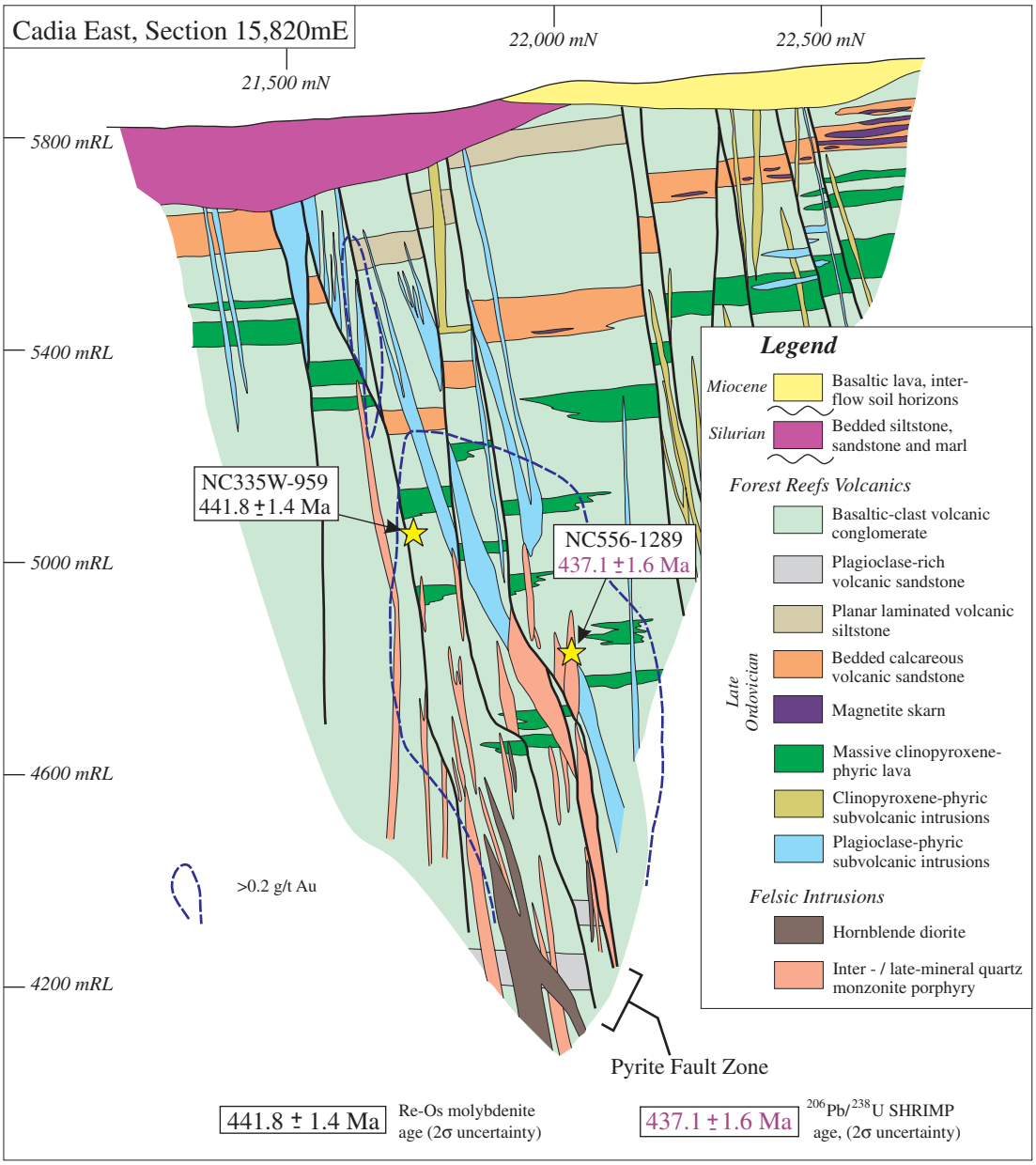

FIG. 9. Re-Os and U-Pb ages from Cadia East, section 15,820mE. Section location is shown in Figure 3. Note that sample NC335W-959 has been projected from ~130 m west of section. Sample NC556-1289 is an intermineral monzonite porphyry (data from Squire, 2001).

1990, 1995; L. Black, 1994, unpub. report for Newcrest Mining Ltd., 14 p.; Glen et al., 2003; Lickfold et al., 2003).

Crosscutting relationships between mineralized veins and the early Late Ordovician Ridgeway Intrusive Complex (456 ± 6 Ma) demonstrate that the Ridgeway ore deposit and associated intrusive complex were coeval (Wilson et al., 2003). Textures supportive of this interpretation include the presence of refractory quartz vein and mineralized wall-rock xenoliths in intermineral intrusions, the truncation of wall-rock–hosted veins at the contact between late mineral intrusions and wall rocks, and the occurrence of porphyry-style mineralization and alteration within the dated intrusive complex (Wilson et al., 2003).

The 456 ± 6 Ma age for the Ridgeway Intrusive Complex is inconsistent with the Ea3 conodont assemblage (449–448 Ma; Cooper, 1999) from the calcareous volcanic sandstone and limestone units at Big Cadia and Little Cadia (Packham et al., 1999; Fig. 3). However, this calcareous lithofacies is absent from the Forest Reefs Volcanics at Ridgeway, supporting the interpretation that the volcanic wall rocks at Ridgeway are a structurally separate domain from those east of the Cadiangullong fault zone (Fig. 3). The age of the Ridgeway Intrusive Complex appears to confirm that movement along this fault zone has juxtaposed different-aged sequences of volcanic rocks, both of which are presently interpreted to be the Forest Reefs Volcanics.

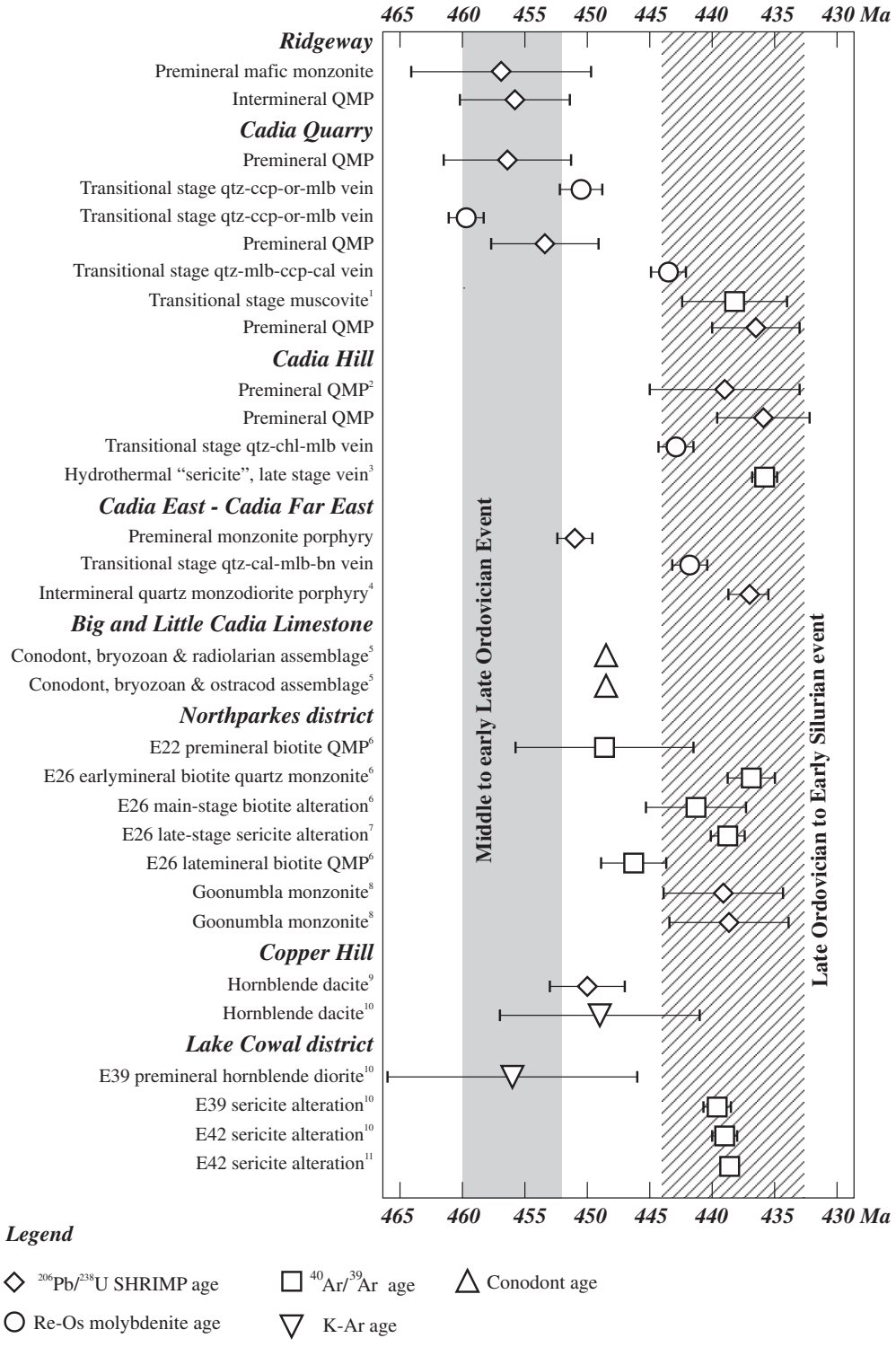

FIG. 10. Summary of the geochronology of the Cadia and surrounding mineral districts. Unless otherwise indicated, samples were analyzed as part of this study. The gray bar represents the approximate age range of the early Late Ordovician intrusive event that produced the Ridgeway Intrusive Complex. Similar-aged intrusions occur both locally at Cadia and regionally at Northparkes, Copper Hill, and Lake Cowal. The crosshatched bar represents a major period of alkalic porphyry gold-copper formation in the Cadia and Northparkes districts, in addition to carbonate-base metal epithermal mineralization at E42/Cowal. Mineral abbreviations: bn = bornite, cal = calcite, ccp = chalcopyrite, chl = chlorite, mlb = molybdenite, or = orthoclase, qtz = quartz. All uncertainties are reported at the 2σ level. Data sources: [1] Forster et al. (2004), [2] L. Black (1994, unpub. report for Newcrest Mining Ltd.), [3] C. Perkins (1994, unpub. report for Newcrest Mining Ltd.), [4] Squire (2001), [5] Packham et al. (1999), [6] Lickfold et al. (2003), [7] Perkins et al. (1990), [8] Butera et al. (2001), [9] Black (1996), [10] Perkins et al. (1995), [11] Miles and Brooker (1998).

At Cadia Quarry and Cadia East, two periods of quartz monzonite porphyry intrusion have been identified (Table 1, Fig. 10). These are an early Late Ordovician event (454 ± 4 Ma) and an Early Silurian event (438 ± 3 Ma). The ages of the older intrusions at Cadia Quarry and Cadia East are indistinguishable from that of the Ridgeway Intrusive Complex, suggesting that the Cadia district experienced a widespread period of intrusive activity at about 455 Ma. The two older molybdenite ages from Cadia Quarry (451 and 460 Ma) overlap the 455 Ma age, thereby indicating that mineralization was also occurring at this time.

In detail at Cadia Quarry, the early Late Ordovician quartz monzonite porphyry occurs immediately to the southwest of the Early Silurian quartz monzonite porphyry (Fig. 6). Most of the porphyry-style mineralization is spatially associated with the younger intrusion. Drill holes that have cut the contact zone between the older and younger quartz monzonite porphyry intrusions (e.g., sample NC 486, Fig. 11) show the older intrusion to contain fewer mineralized quartz veins and a lower gold and copper grade relative to the younger intrusion. The contact is marked by a fault zone that also has juxtaposed the propylitically altered early Late Ordovician quartz monzonite porphyry against a biotite- to sericite-altered, pegmatite-cemented breccia typical of the Cadia Quarry deposit (Fig. 11; Wilson et al., 2004). These relationships are interpreted to indicate that the southwestern limit of the >0.2-g/t Au grade contour marks the trace of a postmineral fault zone that has juxtaposed the 436.5 ± 3.5 Ma intrusion, which hosts the Cadia Quarry orebody, against a weakly mineralized and older (453.4 ± 4.3 Ma) intrusion. This fault may be a previously unrecognized splay of the Cadiangullong fault zone that runs along the southwestern margin of the Cadia Quarry deposit (Fig. 3).

In addition to the intrusive host rocks to the main zone of mineralization at Cadia Quarry and an intermineral quartz monzonite porphyry dike at Cadia East (Squire, 2001), the Early Silurian intrusive event was responsible for a quartz monzonite porphyry intrusion in the center of the Cadia Hill deposit (435.9 ± 3.7 Ma; Fig. 7). An intrusive contact between the Early Silurian quartz monzonite porphyry at Cadia Quarry and the Ea3 (~448 Ma) calcareous volcanic sandstone that hosts the Big Cadia skarn deposit is consistent with the zircon age determination. However, the occurrence of an early Late Ordovician intrusion at Cadia East (NC475-1247, 451 ± 1.4 Ma), less than 400 m beneath the younger Ea3 sandstone horizon, suggests that an as yet unrecognized unconformity surface may exist within the Forest Reefs Volcanics.

Ore formation

The Re-Os data indicate temporally discrete periods of porphyry-related magmatic-hydrothermal activity in the Cadia district during the early Late Ordovician and Early Silurian. The older phase of mineralization is hosted by the ~454 ± 4

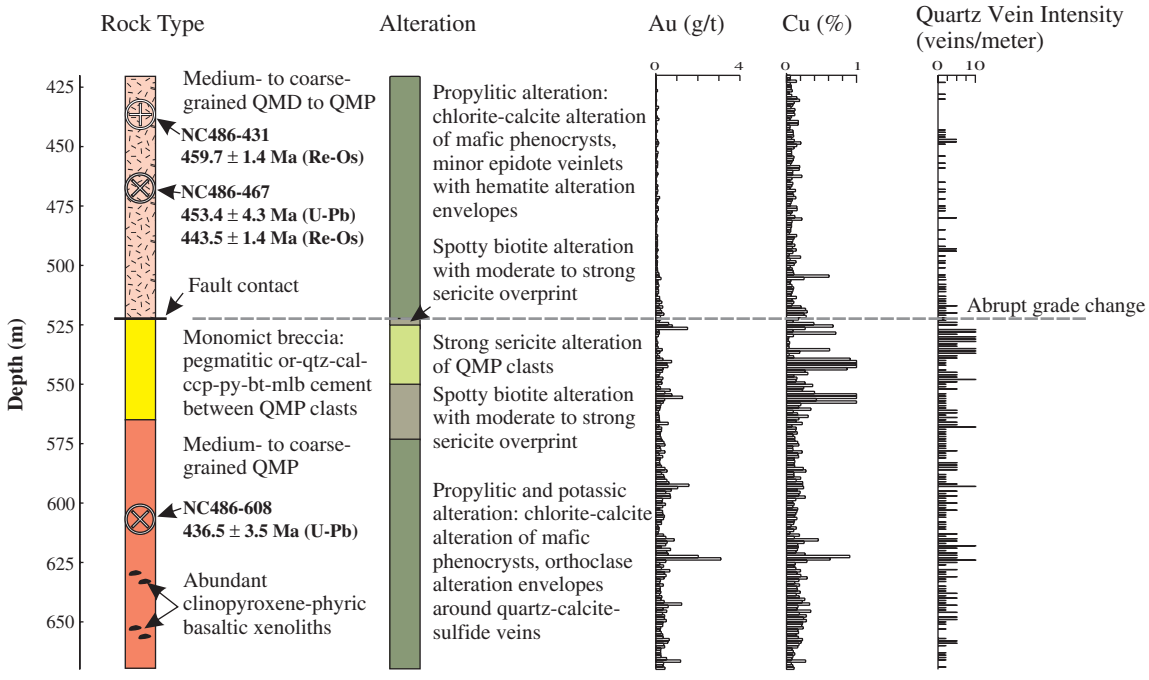

FIG. 11. Geologic drill log, part of sample NC486, Cadia Quarry, showing rock type, alteration, gold and copper grade, and quartz vein density. The location of the drill hole is shown in Figure 6. Multiple intrusive-mineralization events are suggested, based on two $^{206}Pb/^{238}U$ SHRIMP ages and Re-Os molybdenite ages. Evidence supporting an older intrusion in the upper part of the drill hole and a younger intrusion in the lower part includes the presence of brecciated monzonite with a coarse-grained cement of orthoclase-quartz-calcite-chalcopyrite-pyrite-biotite-molybdenite, and an abrupt increase in gold and copper grade (and quartz vein intensity) on passing from the older intrusion into the breccia and underlying younger intrusion. The contact between the breccia and the older intrusion is faulted. The structural juxtaposition of varying styles of alteration on either side of this fault indicates that faulting occurred after alteration and mineralization. Abbreviations: bt = biotite, cal = calcite, ccp = chalcopyrite, mlb = molybdenite, or = orthoclase, py = pyrite, qtz = quartz, QMD = quartz monzodiorite, QMP = quartz monzonite porphyry.

Ma quartz monzonite porphyry intrusion that is situated to the southwest of the main Cadia Quarry deposit (Fig. 4), whereas the younger mineralization is hosted by quartz monzonite porphyry intrusions of similar age and enclosing volcanic wall rocks at Cadia Quarry, Cadia Hill, and Cadia East (Fig. 4).

At Cadia Quarry, at least three temporally discrete events of molybdenite deposition were recorded by the Re-Os data. These events occurred at 459.7 ± 1.4, 450.5 ± 1.7, and 443.5 ± 1.4 Ma (Table 2, Fig. 6) and are hosted by a quartz monzonite porphyry intrusion that has $^{206}Pb/^{238}U$ ages of 453.4 ± 4.3 and 456.4 ± 5.1 Ma. The two older molybdenite samples are within analytical uncertainty of the intrusive age. The youngest molybdenite event appears unrelated to, but nevertheless is hosted by, the 454 Ma intrusion. This younger molybdenite event seen at Cadia Quarry may be related to the quartz monzonite porphyry in the center of the Cadia Quarry orebody (436.5 ± 3.5 Ma). This younger event is also similar to the $^{40}Ar/^{39}Ar$ age of 438.2 ± 5.4 Ma reported for muscovite coexisting with quartz sulfide veins in the center of the Cadia Quarry deposit (Forster et al., 2004), suggesting that the region cooled rapidly after ~440 to 438 Ma.

A similar relationship between the timing of molybdenite crystallization and monzonite intrusion exists at Cadia Hill (Fig. 7). In this deposit, the quartz monzonite porphyry has a $^{206}Pb/^{238}U$ age (435.9 ± 3.7 Ma) that is slightly younger than, and outside analytical uncertainty of, the Re-Os age of a molybdenite-bearing quartz vein (442.9 ± 1.4 and 443.0 ± 1.5 Ma, two separates from same vein). However, the Re-Os molybdenite age is within 2σ uncertainty of the $^{206}Pb/^{238}U$ age of 439 ± 6 Ma for the Cadia Hill quartz monzonite porphyry determined by L. Black (1994, unpub. report for Newcrest Mining Ltd.). At Cadia East, the U-Pb age of the intermineral quartz monzonite porphyry dike (437.1 ± 1.6 Ma: Squire, 2001) is slightly younger than the Re-Os age of molybdenite from a transitional-stage quartz vein (441.8 ± 1.4 Ma); both dike and molybdenite vein occur within the >0.2-g/t Au zone (Fig. 9). These similar ages point to a sequence of temporally close and complex magmatic-hydrothermal events, a feature that is characteristic of the Cadia district (e.g., Wilson et al., 2003) and porphyry systems in general (e.g., Sillitoe, 2000). The consistency of the 443 to 441 Ma Re-Os ages, from three different samples spaced kilometers apart, and representing three different deposits within the district, is significant. Based on the Re-Os data, we conclude that there was a discrete mineralization event at 443 to 441 Ma at Cadia Quarry, Cadia Hill, and Cadia East, and a possibly multistage event at Cadia Quarry between 460 and 450 Ma.

Stein et al. (2001a) noted that Re concentrations in molybdenite can be diagnostic and used to fingerprint multiple events of temporally distinct but spatially overlapping mineralization. For example, two mineralization events were readily apparent at the Archean Boddington gold-copper deposit, Western Australia, on the basis of Re-Os dating of molybdenite (Stein et al., 2001b). The older event produced Re-rich molybdenite (hundreds of ppm Re) and the younger event produced Re-poor molybdenite (<10 ppm Re). The Re concentrations in molybdenite from the two periods of mineralization at Cadia are also markedly different (12 and 25 ppm for the 459–451 Ma molybdenite compared to 170–1,057 ppm for the 443–441 Ma molybdenite), further supporting the interpretation of at least two distinct periods of magmatic-hydrothermal activity in the Cadia district (Table 2, Fig. 12).

The Re-Os and U-Pb age determinations are older than the $^{40}Ar/^{39}Ar$ ages for hydrothermal white mica from Cadia Hill reported by C. Perkins (1994, unpub. report for Newcrest Mining Ltd.). This relationship is consistent with paragenetic observations that the white mica-bearing, late-stage calcite-base metal veins and faults postdate the transitional-stage quartz-calcite-sulfide veins (Wilson, 2002), but perhaps more importantly, the argon spectra are likely to have been disturbed due to episodic thermal activity. Thus, the younger argon ages are considered to record cooling or disturbance and not primary high-temperature magmatic-hydrothermal events. Previous studies have similarly shown that Re-Os ages from other regions are commonly older than $^{40}Ar/^{39}Ar$ and K/Ar data from the same areas, due to resetting of the Ar-Ar system in the magmatic-hydrothermal environment (e.g., Watanabe and Stein, 2000; Stein et al., 2001a; Selby et al., 2002).

The similarity of the estimated ages of intrusion and molybdenite crystallization at Cadia Hill, Cadia East, and the younger portion of Cadia Quarry indicates formation of these porphyry deposits at ~443 to 441 Ma. The weighted average age of the younger molybdenite (442.7 ± 1.6 Ma) is only slightly outside of the 2σ analytical uncertainty of the weighted average age of the younger quartz monzonite porphyry intrusions (437.0 ± 3.8 Ma), and other studies report U-Pb ages (e.g., 439 ± 6 Ma; L. Black, 1994, unpub. report for Newcrest Mining Ltd.) that also overlap the Re-Os results reported here. The older molybdenite ages are interpreted to represent at least two earlier events at ~451 and ~460 Ma and are spatially associated with a ~454 Ma quartz monzonite porphyry intrusion that occupies a position marginal to the main Cadia Quarry orebody. On the basis of geochronology, this interval of intrusive activity and porphyry-style mineralization cannot be distinguished from the event that formed the

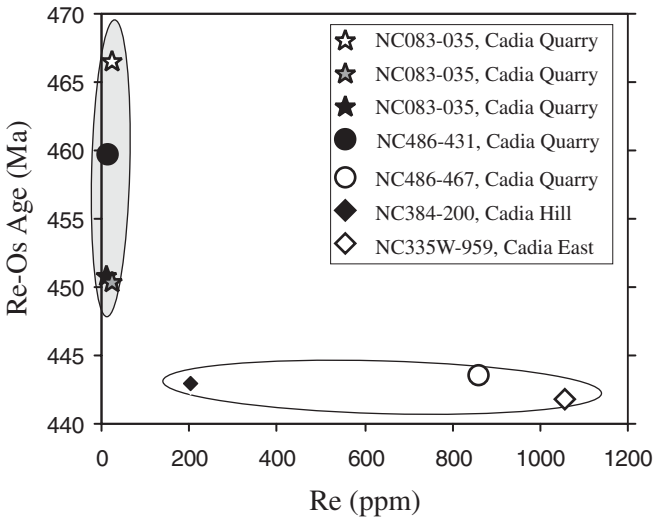

FIG. 12. Re concentrations (ppm) vs. Re-Os ages for molybdenite from the Cadia district (data in Table 2). Older (>450 Ma) molybdenites contain lower Re (<30 ppm), whereas younger (443–441 Ma) molybdenites have higher Re concentrations (>170 ppm).

Ridgeway deposit (~456 Ma). However, the general lack of molybdenite-bearing veins at Ridgeway suggests that it was part of a different system. This implies that several periods of intrusive activity may have occurred in the 460 to 450 Ma interval, in addition to possibly even older, as yet unidentified magmatic-hydrothermal systems.

Implications for Ore Genesis

Temporally discrete magmatic-hydrothermal events

The identification of at least two temporally discrete events of porphyry gold-copper deposit formation within the Cadia district is an important outcome of this study. The 18 m.y. time difference between the formation of the Ridgeway deposit and the other Cadia porphyry deposits is one of the longest recognized time spans for similar porphyry-style mineralization within a single district. Several studies have recognized the occurrence of multiple, temporally discrete events of intrusion and mineralization in porphyry-epithermal districts (e.g., Marsh et al., 1997; Richards et al., 1999; Cannell et al., 2005). The time difference between discrete magmatic-hydrothermal events may range from <2 m.y. (Indio Muerto district, Chile: Gustafson et al., 2001) to about 13 m.y. (Boulder batholith, Montana: Lund et al., 2002). In a recent study of an unmineralized pluton at Yosemite, Coleman et al. (2004) demonstrated, using detailed U-Pb geochronology, that the zoned Tuolumne Intrusive Suite was assembled over a period of about 10 m.y., which led Glazner et al. (2004) to propose that plutons may form incrementally over considerable time periods. A process similar to this may have occurred at midcrustal levels beneath the Cadia district, thereby accounting for the range of U-Pb ages determined throughout the Cadia district.

The Macquarie arc

Alkalic porphyry deposits in the Macquarie arc were previously considered to be of latest Ordovician to Early Silurian age (Perkins et al., 1990, 1995; L. Black, 1994, unpub. report for Newcrest Mining Ltd.; C. Perkins, 1994, unpub. report for Newcrest Mining Ltd.; Lickfold et al., 2003; Fig. 10) related to the Group 4 porphyries of Glen et al. (2003). Early Late Ordovician alkalic gold-copper porphyry deposits had not previously been reported from the Macquarie arc. Butera et al. (2001) previously determined Early Ordovician to Early Silurian ages for shoshonitic monzodiorite to monzonite intrusions in the Northparkes porphyry district (~484, ~451, and ~439 Ma), but intrusions related to porphyry deposit formation were determined to be late Late Ordovician to Early Silurian (~439 Ma). Recent $^{40}Ar/^{39}Ar$ dating of primary biotite phenocrysts from the E26 and E22 porphyry deposits at Northparkes (Lickfold et al., 2003) suggests that magmatic-hydrothermal activity occurred between 446 and 437 Ma, implying that the magmatic-hydrothermal history of the Northparkes district is also more complex than first thought (Fig. 10).

The absolute age of high-sulfidation epithermal deposits of the Macquarie arc (e.g., Peak Hill, Gidginbung; Fig. 2) remains uncertain. The mean $^{40}Ar/^{39}Ar$ age of 409.3 ± 1.9 Ma for sericite at Peak Hill was interpreted by Perkins et al. (1995) to be a deformation age, thereby constraining the minimum age of this deposit. Similarly young $^{40}Ar/^{39}Ar$ ages (417.3 ± 2.0 and 401.2 ± 2.0 Ma) from deformed alunite at Gidginbung were considered to represent cooling through chronometer closure temperatures, rather than a measure of the age of mineralization (Perkins et al., 1995). More recent attempts to date zircons of interpreted hydrothermal origin that occur in the Gidginbung advanced argillic alteration assemblage (Mernagh et al., 2004) have returned a weighted mean $^{206}Pb/^{238}U$ age of 436.4 ± 3.1 Ma (Lawrie et al., 2007). Similar $^{40}Ar/^{39}Ar$ ages have been determined for sericite from porphyry and epithermal mineralization in the Cowal district (439.9 ± 1.1 Ma at E39 and 439.0 ± 1.0 Ma at E42: Perkins et al., 1995; Miles and Brooker, 1998), gold skarn mineralization at Junction Reefs (439.3 ± 2.0 Ma: Perkins et al., 1995), and muscovite at Cadia Quarry (438.2 ± 5.4 Ma: Forster et al., 2004).

These ages are collectively indicative of a widespread latest Ordovician to Early Silurian magmatic-hydrothermal event throughout the Macquarie arc that produced porphyry, skarn, and epithermal mineralization. Although volcanic and intrusive rocks of Middle to Late Ordovician age are widespread throughout the Macquarie arc (Glen et al., 2003), the 456 ± 6 Ma Ridgeway Intrusive Complex is currently the only known example of early Late Ordovician igneous rocks genetically linked to high-grade gold-copper mineralization.

Tectonic implications

Multiple events of magmatic-hydrothermal activity require the episodic release of fertile magmas and structural conditions that would have been favorable for the repeated ascent and trapping of the ore-forming melt. At Cadia, this occurred at least twice in essentially the same location, 18 m.y. apart.

Shoshonitic igneous rocks, such as those that host mineralization at Cadia (Blevin, 2002; Holliday et al., 2002), are not the typical products of arc magmatism, comprising only about 2.5 vol percent of igneous rocks in circum-Pacific volcanic arc terranes (Baker, 1982). In modern volcanic arcs, shoshonites typically occur either further from the subduction zone than contemporaneous tholeiitic and medium K calc-alkalic rocks (e.g., southern Andes: Déruelle, 1978; Sunda arc: Whitford and Nicholls, 1976) or as linear arrays of volcanic centers on cross-arc extensional structures (e.g., Fiji: Gill and Whelan, 1989; northern Mariana arc: Stern et al., 1988). Extensional structures are interpreted to tap deeper, more enriched parts of the mantle (Bloomer et al., 1989) and allow small degrees of partial melting of a depleted mantle that has been recently modified by subduction processes (Gill and Whelan, 1989).

At Cadia, shoshonitic intrusions and related hydrothermal alteration are focused within a 6-km-long, west-northwest–trending corridor (Fig. 3) that is oriented transverse to the interpreted strike of the Macquarie arc (Glen et al., 1998). This corridor is parallel to and lies within the west-northwest–trending Lachlan transverse zone, which has been proposed to be a lineament that transects the Lachlan fold belt and may be an extension of a major trans-Australia cratonic structure (Glen and Walshe, 1999). The genesis of shoshonitic melts at Cadia is postulated to have occurred in response to local extension that developed as a result of district-scale dextral strike-slip motion along structures parallel to the Lachlan transverse zone (Wilson, 2003). At Cadia East, for example, the mineralizing intrusions have been emplaced within a

downdropped block of Forest Reefs Volcanics country rock (Tedder et al., 2001), suggesting local extension. These extensional structures apparently tapped a deep, subduction-modified, depleted mantle source. Melts may have utilized these structures to ascend to high crustal levels as small fingerlike bodies, leading to low-pressure fractionation of plagioclase, clinopyroxene, apatite, and titanite, and hydrothermal alteration and mineralization in response to the exsolution of a magmatic aqueous phase (Wilson et al., 2003).

Conclusions

The gold-copper porphyry deposits of the Cadia district formed in two mineralizing episodes separated by 18 m.y., from the Late Ordovician to Early Silurian. Intrusions intimately related to the Ridgeway orebody were emplaced at 456 ± 6 Ma, as were weakly mineralized intrusions at Cadia Quarry and Cadia East (454 ± 4 Ma). Re-Os molybdenite ages of 459.7 ± 1.4 and 450.8 ± 1.4 Ma from Cadia Quarry indicate that at least some porphyry-style mineralization was associated with intrusions between 460 and 450 Ma. A second episode of intrusive activity occurred at 437 ± 4 Ma, based on a $^{206}Pb/^{238}U$ weighted average age for quartz monzonitic stocks and dikes that host mineralization in Cadia Quarry, Cadia Hill, and Cadia East. Re-Os molybdenite ages from these deposits range from 443.5 ± 1.4 to 441.8 ± 1.4 Ma, indicating that mineralization was widespread over a narrow period of time contemporaneous with intrusive activity. The styles of mineralization and alteration in both episodes are similar, although the Re contents of molybdenite produced by the two events are different.

Alkalic porphyry gold-copper deposits in the Macquarie arc are not restricted in time to the ~440 to 438 Ma period as previously thought (Perkins et al., 1990, 1995; Glen et al., 2003). Rather, high-grade mineralization also occurred in association with shoshonitic intrusions emplaced at ~460 to 450 Ma. The occurrence of economically significant gold-copper mineralization with intrusions of markedly different ages should be an important consideration when exploring the Macquarie arc.

Acknowledgments

This work was generously supported and funded by Newcrest Mining Ltd. and the Centre for Ore Deposit Research. Many geologists have contributed to the understanding of the geology of the Cadia district and we would like to thank them all. Newcrest Mining Ltd. is also thanked for permission to publish this paper and for funding the publication of color figures. Part of the Re-Os study was generously supported by NSF grant EAR-0087483 to Holly Stein. CODES is the Australian Research Council's Centre for Excellence in Ore Deposit Research. The authors would also like to thank *Economic Geology* reviewers Eric Seedorff, Ryan Morelli, and Mark Hannington for their thorough, helpful, and constructive comments.

March 13, September 19, 2006

REFERENCES

Ambler, E.P., Cooper, J., and Howards, P.F., 1977, A radiometric age of intrusion and hydrothermal alteration at Cadia, NSW: Search, v. 8, p. 244–246.

Arribas, A., Hedenquist, J.W., Itaya, T., Okada, T., Concepcion, R.A., and Garcia, J.S., Jr., 1995, Contemporaneous formation of adjacent porphyry and epithermal Cu-Au deposits over 300 ka in northern Luzon, Philippines: Geology, v. 23, p. 337–340.

Baker, P.E., 1982, Evolution and classification of orogenic volcanic rocks, *in* Thorpe, R.S., ed., Andesites: Orogenic andesites and related rocks: Chichester, NY, John Wiley and Sons, p. 11–23.

Bastrakov, E.N., Brooker, M., and Walshe, J.L., 1996, The origin of gold mineralisation at Lake Cowal, Endeavour 42 (NSW) [abs.]: Australian Geological Convention, 13th, Geological Society of Australia Abstracts, v. 41, p. 23.

Blevin, P.L., 2002, The petrographic and compositional character of variably K-enriched magmatic suites associated with Ordovician porphyry Cu-Au mineralisation in the Lachlan fold belt, Australia: Mineralium Deposita, v. 37, p. 87–99.

Bloomer, S.H., Stern, R.J., Fisk, E., and Geschwind, C.H., 1989, Shoshonitic volcanism in the northern Mariana Arc I. Mineralogic and major and trace element characteristics: Journal of Geophysical Research, v. 94, p. 4469–4496.

Butera, K.M., Williams, I.S., Blevin, P.L., and Simpson, C.J., 2001, Zircon U-Pb dating of Early Palaeozoic monzonitic intrusives from the Goonumbla area, New South Wales: Australian Journal of Earth Sciences, v. 48, p. 457–464.

Bywater, A., Williams, S., McInnes, P., and Dijkmans, V., 2004, Developments at the Cowal gold project [abs.]: Geological Society of Australia Abstracts, v. 74, p. 77–82.

Cannell, J., Cooke, D., Walshe, J., and Stein, H., 2005, Geology, mineralization, alteration, and structural evolution of the El Teniente porphyry Cu-Mo deposit: Economic Geology, v. 100, p. 979–1003.

Carr, G.R., Dean, J.A., Suppel, D.W., and Heithersay, P.S., 1995, Precise lead isotope fingerprinting of hydrothermal activity associated with Ordovician to Carboniferous metallogenic events in the Lachlan fold belt of New South Wales: Economic Geology, v. 90, p. 1467–1505.

Cas, R.A.F., VandenBerg, A.H.M., Allen, R.L., Clifford, B.A., Fergusson, C.L., Morand, V. J., and Stewart, I.R., 1988, Ordovician, *in* Douglas, J.G., and Ferguson, J.A., eds., Geology of Victoria: Victorian Division, Melbourne, Victoria, Australia, Geological Society of Australia, p. 63–102.

Coleman, D.S., Gray, W., and Glazner, A.F., 2004, Rethinking the emplacement and evolution of zoned plutons: Geochronologic evidence for incremental assembly of the Tuolumne Intrusive Suite, California: Geology, v. 32, p. 433–436.

Collins, W.J., and Vernon, R.H., 1992, Palaeozoic arc growth, deformation and migration across the Lachlan fold belt, southeastern Australia: Tectonophysics, v. 214, p. 381–400.

Compston, W., Williams, I.S., Kirschvink, J.L., Zichao, Z., and Guogan, M., 1992, Zircon U-Pb ages for the Early Cambrian time-scale: Journal of the Geological Society of London, v. 149, p. 171–184.

Cooper, R.A., 1999, The Ordovician timescale—calibration of graptolite and conodont zones: Acta Universitaris Carolinae, v. 43, p. 1–4.

Corbett, G.J., and Leach, T.M., 1998, Southwest Pacific rim gold-copper systems: Structure, alteration and mineralization: Society of Economic Geologists Special Publication 6, 237 p.

Degeling, P.R., Corbett, G.J., and Leach, T.M., 1995, The Peak Hill high sulphidation gold deposit, NSW: Parkville, Victoria, Australia, Australasian Institute of Mining and Metallurgy Publication Series, v. 9, p. 175–180.

Déruelle, B., 1978, Calc-alkaline and shoshonitic lavas from five Andean volcanoes (between latitudes 21°45' and 24°30'S) and the distribution of the Plio-Quaternary volcanism of the south-central and southern Andes: Journal of Volcanology and Geothermal Research, v. 3, p. 281–298.

Forster, D.B., Seccombe, P.K., and Phillips, D., 2004, Controls on skarn mineralization and alteration at the Cadia deposits, New South Wales, Australia: Economic Geology, v. 99, p. 761–788.

Garwin, S.L., 2000, The setting, geometry and timing of intrusion-related hydrothermal systems in the vicinity of the Batu Hijau porphyry copper-gold deposit, Sumbawa, Indonesia: Unpublished Ph.D. thesis, Perth,University of Western Australia, 452 p.

Gill, J., and Whelan, P., 1989, Early rifting of an oceanic island arc (Fiji) produced shoshonitic to tholeiitic basalts: Journal of Geophysical Research, v. 94, p. 4561–4578.

Glazner, A.F., Bartley, J.M., Coleman, D.S, Gray, W., and Taylor, R.Z, 2004, Are plutons assembled over millions of years by amalgamation from small magma chambers?: GSA Today, v. 14, p. 4–11.

Glen, R.A., and Walshe, J.L., 1999, Cross-structures in the Lachlan orogen: the Lachlan transverse zone example: Australian Journal of Earth Sciences, v. 46, p. 641–658.

Glen, R.A., Walshe, J.L., Barron, L.M., and Watkins, J.J., 1998, Ordovician convergent-margin volcanism and tectonism in the Lachlan sector of East Gondwana: Geology, v. 26, p. 751–754.

Glen, R.A., Korsch, R.J., Direen, N.G., Jones, L.E.A., Johnstone, D.W., Lawrie, K.C., Finlayson, D.M., and Shaw, R.D., 2002, Crustal structure of the Ordovician Macquarie arc, eastern Lachlan orogen, based on seismic-reflection profiling: Australian Journal of Earth Sciences, v. 49, p. 323–348.

Glen, R.A., Crawford, A.J., and Cooke, D.R., 2003, Tectonic setting of porphyry copper-gold mineralisation in the Macquarie arc: North Ryde, New South Wales, Australia, Australian Geological Survey Organisation Report 2003/14, p. 65–68.

Gray, N., Mandyczewsky, A., and Hine, R., 1995, Geology of the zoned gold skarn system at Junction reefs, New South Wales: ECONOMIC GEOLOGY, v. 90, p. 1533–1552.

Green, D., 1999, Geology, geochemistry and genesis of the Big Cadia deposit, N.S.W.: Unpublished B.Sc. Honours thesis, Hobart, University of Tasmania, 187 p.

Gustafson, L.B., Orquera, W., McWilliams, M., Castro, M., Olivares, O., Rojas, G., Maluenda, J., and Mendez, M., 2001, Multiple centers of mineralization in the Indio Muerto district: ECONOMIC GEOLOGY, v. 96, p. 325–350.

Harris, A.C., Allen, C.M., Bryan, S.E., Campbell, I.H., Holcombe, R.J., and Palin, J.M., 2004, ELA-ICP-MS U-Pb zircon geochronology of regional volcanism hosting the Bajo de la Alumbrera Cu-Au deposit: Implications for porphyry-related mineralization: Mineralium Deposita, v. 39, p. 46–67.

Heithersay, P.S., and Walshe, J.L., 1995, Endeavour 26 North: A porphyry copper-gold deposit in the Late Ordovician, shoshonitic Goonumbla volcanic complex, New South Wales, Australia: ECONOMIC GEOLOGY, v. 90, p. 1506–1532.

Heithersay, P.S., O'Neill, W.J., van der Helder, P. , Moore, C.R., and Harbon, P.G., 1990, Goonumbla porphyry copper district—Endeavour 26 North, Endeavour 22 and Endeavour 27 copper-gold deposits: Australasian Institute of Mining and Metallurgy Monograph 14, v. 2, p. 1385–1398.

Holliday, J.R., Wilson, A.J., Blevin, P.L., Tedder, I.J., Dunham, P.D., and Pfitzner, M., 2002, Porphyry gold-copper mineralisation in the Cadia district, eastern Lachlan fold belt, New South Wales and its relationship to shoshonitic magmatism: Mineralium Deposita, v. 37, p. 100–116.

Lawrie, K.C., Mernagh, T.P. , Ryan, C.G., Van Achterberg, E., and Black, L., 2007, Chemical fingerprinting of hydrothermal zircons: An example from the Gidginbung high sulphidation Au-Ag-(Cu) deposit, New South Wales: Proceedings of the Geologists Association, v. 118, p. 37–46.

Lickfold, V., Cooke, D.R., Smith, S.G., and Ullrich, T.D., 2003, Endeavour copper-gold porphyry deposits, Northparkes, New South Wales: Intrusive history and fluid evolution: ECONOMIC GEOLOGY, v. 98, p. 1607–1636.

Ludwig, K.R., 2001, SQUID 1.02, A user's manual: Berkeley, California, Berkeley Geochronology Center Special Publication 2, 71 p.

———2003, Isoplot/Ex version 3.0: A geochronological toolkit for Microsoft Excel: Berkeley, California, Berkeley Geochronology Center Special Publication 4.

Lund, K., Aleinikoff, J.N., Kunk, M.J., Unruh, D.M., Zeihen, G.D., Hodges, W.C., Du Bray, E.A., and O'Neill, J.M., 2002, SHRIMP U-Pb and $^{40}Ar/^{39}Ar$ age constraints for relating plutonism and mineralization in the Boulder batholith region, Montana: ECONOMIC GEOLOGY, v. 97, p. 241–267.

Markey, R.J., Stein, H.J., and Morgan, J.W., 1998, Highly precise Re-Os dating of molybdenite using alkaline fusion and NTIMS: Talanta, v. 45, p. 935–946.

Markey, R.J., Hannah, J.L., Morgan, J.W., and Stein, H.J., 2003, A double spike for osmium analysis of highly radiogenic samples: Chemical Geology, v. 200, p. 395–406.

Marsh, T.M., Einaudi, M.T., and McWilliams, M., 1997, $^{40}Ar/^{39}Ar$ geochronology of Cu-Au and Au-Ag mineralization in the Potrerillos district, Chile: ECONOMIC GEOLOGY, v. 92, p. 784–806.

Masterman, G.J., White, N.C., Wilson, C.J.L., and Pape, D., 2002, High-sulfidation gold deposits in ancient volcanic terranes: Insights from the mid-Paleozoic Peak Hill deposit, NSW: Society of Economic Geologists Newsletter 51, p. 1–16.

Mernagh, T.P., Lawrie, K.C., Belousova, E.A., van Achterbergh, E., and Ryan, C.G., 2004, The identification of hydrothermal zircons in mineral deposits: Centre for Global Metallogeny, University of Western Australia Publication 33, p. 444–447.

Miles, I.N., and Brooker, M.R., 1998, Endeavour 42 deposit, Lake Cowal, New South Wales: A structurally controlled gold deposit: Australian Journal of Earth Sciences, v. 45, p. 837–847.

Müller, D., Rock, N.M.S., and Groves, D.I., 1992, Geochemical discrimination between shoshonitic and potassic volcanic rocks from different tectonic settings: A pilot study: Mineralogy and Petrology, v. 46, p. 259–289.

Paces, J.B., and Miller, J.D., 1993, Precise U-Pb ages of the Duluth Complex and related mafic intrusions, northeastern Minnesota: Geochronological insights to physical, petrogenetic, paleomagnetic and tectonomagmatic process associated with the 1.1 Ga Midcontinent rift system: Journal of Geophysical Research, v. 98, p. 13,997–14,013.

Packham, G.H., 1987, The eastern Lachlan fold belt of Southeast Australia: A possible Late Ordovician to Early Devonian sinistral strike slip regime: Geodynamics Series 19, p. 67–82.

Packham, G., Percival, I., and Bischoff, G., 1999, Age constraints on strata enclosing the Cadia and Junction reefs ore deposits of central New South Wales and tectonic implications: Geological Survey of New South Wales, Quarterly Notes, v. 110, p. 1–12.

Perkins, C., McDougall, I., Claoue, L.J., and Heithersay, P.S., 1990, $^{40}Ar/^{39}Ar$ and U-Pb geochronology of the Goonumbla porphyry Cu-Au deposits, New South Wales, Australia: ECONOMIC GEOLOGY, v. 85, p. 1808–1824.

Perkins, C., McDougall, I., and Walshe, J.L., 1992, Timing of shoshonitic magmatism and gold mineralisation, Sheahan-Grants and Glendale, New South Wales: Australian Journal of Earth Sciences, v. 39, p. 99–110.

Perkins, C., Walshe, J.L., and Morrison, G., 1995, Metallogenic episodes of the Tasman fold belt system, eastern Australia: ECONOMIC GEOLOGY, v. 90, p. 1443–1466.

Pogson, D.J., and Watkins, J.J., 1998, Bathurst 1:250 000 geological sheet SI/55–8: Explanatory Notes: Sydney, Australia, Geological Survey of New South Wales, 430 p.

Richards, J.P., Noble, S.R., and Pringle, M.S, 1999, A revised late Eocene age of porphyry Cu magmatism in the Escondida area: ECONOMIC GEOLOGY, v. 94, p. 1231–1247.

Richardson, S., 1976, Geology and mineralization of the Cargo area: International Geological Congress, Ore Deposits of the Lachlan fold belt, New South Wales, Sydney, Proceedings, p. 10–12.

Richardson, S.J., Bowman, H.N., Paterson, I.B.L., and Hobbs, J.J., 1983, Late Silurian to Early Devonian porphyry copper-gold-molybdenum deposits: Disseminated copper-gold mineralization at Cargo: Sydney, N.S.W., Australia, Records of the Geological Survey of New South Wales 21, p. M29–M51.

Scheibner, E., 1973, A plate tectonic model of the Palaeozoic tectonic history of New South Wales: Journal of the Geological Society of Australia, v. 20, p. 405–426.

Scheibner, E., and Basden, H., 1998, Geology of New South Wales—synthesis volume 2. Geological evolution: Sydney, New South Wales Geological Survey, 666 p.

Scheibner, E., and Veevers, J.J., 2000, Tasman fold belt system, *in* Veevers, J.J., ed., Billion-year earth history of Australia and neighbours in Gondwanaland: Sydney, Geochemical Evolution and Metallogeny of Continents (GEMOC) Press, Macquarie University, p. 154–234.

Scott, K.M., 1976, The geochemistry of the Copper Hill deposit: Bulletin of the Australian Society of Exploration Geophysicists, v. 7, p. 30–31.

——1978, Geochemical aspects of the alteration-mineralization at Copper Hill, New South Wales, Australia: ECONOMIC GEOLOGY, v. 73, p. 966–976.

Selby, D., Creaser, R.A., Hart, C.J.R., Rombach, C.S., Thompson, J.F.H., Smith, M.T., Bakke, A.A., and Goldfarb, R.J., 2002, Absolute timing of sulfide and gold mineralization: A comparison of Re-Os molybdenite and Ar-Ar mica methods from the Tintina gold belt, Alaska: Geology, v. 30, p. 791–794.

Shirey, R.B., and Walker, R.J., 1995, Carius-tube digestion for low-blank Re-Os analysis: Analytical Chemistry, v. 34, p. 2136–2141.

Sillitoe, R.H., 2000, Gold-rich porphyry deposits: Descriptive and genetic models and their role in exploration and discovery: Reviews in Economic Geology, v. 13, p. 315–345.

Smoliar, M.I., Walker, R.J., and Morgan, J.W., 1996, Re-Os ages of group IIA, IIIA, IVA and IVB iron meteorites: Science, v. 271, p. 1099–1102.

Squire, R.J., 2001, Volcanological and tectono-magmatic evolution of the Cadia-Neville region, NSW: Unpublished Ph.D. thesis, University of Tasmania, 221 p.

Stein, H.J., 2006, Low-rhenium molybdenite by metamorphism in northern Sweden: Recognition, genesis, and global implications: Lithos, v. 87, p. 300–327.

Stein, H.J., Scherstén, A., Hannah, J., and Markey, R., 2003, Sub-grain scale decoupling of Re and ^{187}Os and assessment of laser ablation ICP-MS spot dating in molybdenite: Geochimica et Cosmochimica Acta, v. 67, p. 3673–3686.

Stein, H.J., Markey, R.J., Morgan, J.W., Du, A., and Sun, Y., 1997, Highly precise and accurate Re-Os ages for molybdenite from the East Qinling molybdenum belt, Shaanxi province, China: ECONOMIC GEOLOGY, v. 92, p. 827–835.

Stein, H.J., Markey, R.J., Morgan, J.W., Hannah, J.L., and Scherstén, A., 2001a, The remarkable Re-Os chronometer in molybdenite: How and why it works: Terra Nova, v. 13, p. 479–486.

Stein, H.J., Markey, R.J., Morgan, J.W., Selby, D., Creaser, R.A., McCuaig, T.C., and Behn, M., 2001b, Re-Os dating of Boddington molybdenite, SW Yilgarn: Two Au mineralization events: Australian Geological Survey Organisation-Geoscience Australia Record, v. 37, p. 469–471.

Stern, R.J., Bloomer, S.H., Ping-Nan, L., Ito, E., and Morris, J., 1988, Shoshonitic magmas in nascent arc: New evidence from submarine volcanoes in the northern Marianas: Geology, v. 16, p. 426–430.

Tedder, I.J., Holliday, J., and Hayward, S., 2001, Discovery and evaluation drilling of the Cadia Far East gold-copper deposit: NewGen Gold 2001, Case Histories of Discovery: Perth, Australian Mineral Foundation, p. 171–184.

Tera, F., and Wasserburg, G., 1972, U-Th-Pb systematics in three Apollo 14 basalts and the problem of initial Pb in lunar rocks: Earth and Planetary Science Letters, v. 14, p. 281–304.

Thompson, J.F.H., Lessman, J., and Thompson, A.J.B., 1986, The Temora gold-silver deposit: A newly recognized style of high sulfur mineralization in the lower Paleozoic of Australia: Economic Geology, v. 81, p. 732–738.

Watanabe, Y., and Stein, H.J., 2000, Re-Os ages for the Erdenet and Tsagaan Suvarga porphyry Cu-Mo deposits, Mongolia, and tectonic implications: Economic Geology, v. 95, p. 1537–1542.

Watanabe, Y., Stein, H.J., Morgan, J.W., and Markey, R.J., 1999, Re-Os geochronology brackets timing and duration of mineralization for the El Salvador porphyry Cu-Mo deposit, Chile [abs.]: Geological Society of America Abstracts with Programs, v. 31, p. A-30.

Wellman, P., and McDougall, I., 1974, Potassium-argon ages on Cainozoic volcanic rocks of New South Wales: Geological Society of Australia Journal, v. 21, p. 247–272.

Whitford, D.J., and Nicholls, I.A., 1976, Potassium variation in lavas across the Sunda arc in Java and Bali, *in* Johnson, R.W., ed., Volcanism in Australasia: Amsterdam, Elsevier, p. 63–76.

Williams, I.S., 1998, U-Th-Pb geochronology by ion microprobe: Reviews in Economic Geology, v. 7, p. 1–35.

Wilson, A.J., 2002, Diverse styles of porphyry gold-copper mineralisation, Cadia district, New South Wales, Australia [abs.]: Giant Ore Deposits, Centre for Ore Deposit Research, University of Tasmania, Hobart, Abstract Volume, p. 29–31.

——2003, The geology, genesis and exploration context of the Cadia gold-copper porphyry deposits, NSW, Australia: Unpublished Ph.D. thesis, Hobart, University of Tasmania, 335 p.

Wilson, A.J., Cooke, D.R., Holliday, J.R., and Tedder, I.J., 2002, The Cadia gold-copper district, New South Wales: Geology and discovery: Vancouver, BC, Vancouver Mining and Exploration Group, British Columbia and Yukon Chamber of Mines, 4 p.

Wilson, A.J., Cooke, D.R., and Harper, B.L., 2003, The Ridgeway gold-copper deposit: A high-grade alkalic porphyry deposit in the Lachlan fold belt, New South Wales, Australia: Economic Geology, v. 98, p. 1637–1666.

Wilson, A.J., Cooke, D.R., and Richards, T., 2004, Veins, pegmatites and breccias: Examples from the alkalic Cadia Quarry gold-copper porphyry deposit, NSW, Australia: Hobart, Australia, Centre for Ore Deposit Research (CODES) Special Publication 5, p. 45–55.

Wyborn, D., and Sun, S.S., 1993, Nd-isotopic "fingerprinting" of Cu/Au mineralisation in the Lachlan fold belt: Australian Geological Survey Organisation Research Newsletter 19, p. 13–14.

APPENDIX

Summary of SHRIMP U-Pb Zircon and Titanite Data (in all tables, - = no ^{204}Pb detected)

Sample NC498-569. Ridgeway Intrusive Complex premineralization mafic monzonite
Drill hole NC498, depth 569.0 m, AMG coordinates (AGD84 datum), 683552E, 6298410N

	Titanite analyses						Total				Radiogenic		Age (Ma)	
Grain spot	U (ppm)	Th (ppm)	Th/U	^{206}Pb* (ppm)	^{204}Pb/ ^{206}Pb	f_{206} %	^{238}U/ ^{206}Pb	±1σ	^{207}Pb/ ^{206}Pb	±1σ	^{206}Pb/ ^{238}U	±1σ	^{206}Pb/ ^{238}U	±1σ
1.1	12	77	6.51	0.8	0.008853	16.0	12.325	0.433	0.1798	0.0038	0.0687	0.0025	428.0	14.9
2.1	30	135	4.54	2.1	0.005200	9.3	12.114	0.280	0.1348	0.0025	0.0746	0.0018	463.5	10.6
3.1	169	878	5.19	11.1	0.001125	2.0	13.130	0.184	0.0714	0.0006	0.0747	0.0011	464.7	6.4
4.1	129	234	1.81	8.1	0.000677	1.2	13.692	0.203	0.0661	0.0007	0.0721	0.0011	448.9	6.5
5.1	19	263	13.99	1.4	0.005882	10.6	11.760	0.317	0.1360	0.0026	0.0767	0.0021	476.4	12.7
6.1	10	114	11.31	0.9	0.011850	21.3	10.128	0.505	0.2551	0.0046	0.0746	0.0038	463.6	22.9
7.1	12	142	12.01	0.9	0.008266	14.9	11.654	0.382	0.1797	0.0053	0.0727	0.0025	452.5	14.9
8.1	4	19	5.42	0.4	0.021921	39.3	7.832	0.462	0.3833	0.0192	0.0763	0.0055	474.0	32.9
9.1	7	42	5.94	0.6	0.011959	21.5	10.611	0.428	0.2569	0.0049	0.0709	0.0030	441.4	17.8
10.1	33	4	0.13	2.2	0.001626	2.9	13.054	0.299	0.0823	0.0016	0.0741	0.0017	461.1	10.4
10.2	19	231	12.32	2.6	0.029369	52.7	6.217	0.173	0.4698	0.0165	0.0790	0.0040	490.0	23.9
11.1	15	258	17.43	1.0	0.006662	12.0	12.098	0.356	0.1649	0.0043	0.0715	0.0022	445.4	13.1
*12.1	25	148	5.96	1.5	0.003888	7.0	14.007	0.339	0.1115	0.0020	0.0664	0.0016	414.5	9.9
13.1	17	89	5.07	1.3	0.006975	12.5	11.515	0.375	0.1639	0.0041	0.0753	0.0025	468.2	15.1
*excluded spot		Single population, 13 spots					MSWD = 1.14				Weighted mean		456.9	7.2

Sample NC498-809. Ridgeway Intrusive Complex inter/late mineralization quartz monzonite porphyry
Drill hole NC498, depth 808.8 m, AMG coordinates (AGD84 datum), 683620E, 6298503N

	Zircon analyses						Total				Radiogenic		Age (Ma)	
Grain spot	U (ppm)	Th (ppm)	Th/U	^{206}Pb* (ppm)	^{204}Pb/ ^{206}Pb	f_{206} %	^{238}U/ ^{206}Pb	±1σ	^{207}Pb/ ^{206}Pb	±1σ	^{206}Pb/ ^{238}U	±1σ	^{206}Pb/ ^{238}U	±1σ
1.1	91	32	0.03	5.8	0.000534	0.64	13.55	0.16	0.0613	0.0010	0.0733	0.0009	456.1	5.4
2.1	167	49	0.29	10.6	0.000512	0.48	13.54	0.17	0.0600	0.0007	0.0735	0.0009	457.3	5.6
3.1	184	55	0.30	11.5	0.000192	0.28	13.67	0.15	0.0583	0.0007	0.0729	0.0008	453.9	4.8
4.1	301	116	0.38	19.0	0.000145	0.20	13.62	0.14	0.0577	0.0005	0.0733	0.0008	455.9	4.5
*5.1	151	55	0.36	9.6	0.007312	13.03	13.52	0.90	0.1601	0.0163	0.0643	0.0046	401.9	28.0
*6.1	106	42	0.40	7.3	0.002675	5.47	12.46	0.22	0.1008	0.0112	0.0759	0.0018	471.4	11.0
7.1	310	132	0.43	19.6	0.000188	0.23	13.63	0.14	0.0580	0.0008	0.0732	0.0008	455.4	4.6
*8.1	109	39	0.36	7.2	0.000199	0.56	13.10	0.15	0.0610	0.0010	0.0759	0.0009	471.7	5.5
8.2	141	50	0.36	9.0	0.000868	1.91	13.51	0.15	0.0715	0.0028	0.0726	0.0009	452.0	5.1
*9.1	186	70	0.37	11.4	0.000308	0.15	14.10	0.15	0.0569	0.0007	0.0708	0.0008	440.9	4.6
10.1	112	38	0.34	7.0	-	0.25	13.62	0.21	0.0581	0.0009	0.0732	0.0011	455.5	6.8
*11.1	109	36	0.33	7.1	0.000621	0.71	13.14	0.15	0.0622	0.0011	0.0756	0.0009	469.9	5.3
12.1	242	107	0.44	15.2	0.000153	0.31	13.69	0.14	0.0586	0.0006	0.0728	0.0008	453.1	4.5
13.1	90	29	0.32	5.6	0.000181	0.65	13.78	0.19	0.0611	0.0010	0.0721	0.0010	448.6	6.1
14.1	201	81	0.40	13.0	0.000245	0.47	13.31	0.14	0.0601	0.0007	0.0748	0.0008	465.0	4.8
15.1	205	77	0.38	12.8	0.000093	0.23	13.80	0.14	0.0578	0.0006	0.0723	0.0008	449.8	4.6
16.1	151	66	0.44	9.5	0.000242	0.35	13.59	0.15	0.0589	0.0008	0.0733	0.0008	456.2	4.9
16.2	114	36	0.32	7.4	0.000542	0.54	13.28	0.15	0.0607	0.0009	0.0749	0.0009	465.5	5.2
17.1	101	36	0.35	6.4	0.000508	0.56	13.58	0.16	0.0606	0.0010	0.0732	0.0009	455.5	5.2
18.1	302	102	0.34	19.2	0.000248	<0.01	13.49	0.14	0.0561	0.0005	0.0742	0.0008	461.2	4.5
19.1	431	158	0.37	27.7	0.000064	0.09	13.38	0.13	0.0570	0.0004	0.0747	0.0007	464.3	4.4
20.1	127	42	0.33	7.8	0.000326	0.62	13.95	0.17	0.0608	0.0009	0.0712	0.0009	443.6	5.3
21.1	324	139	0.43	20.5	0.000069	0.06	13.57	0.16	0.0567	0.0005	0.0737	0.0009	458.2	5.3
22.1	208	88	0.42	13.0	0.000283	0.46	13.77	0.15	0.0597	0.0007	0.0723	0.0008	449.8	4.7
*excluded spots		Single population, 19 spots					MSWD = 1.30				Weighted mean		455.8	4.4

The sample stage moved during the analyses of zircons 5.1 and 6.1; data presented for information purposes only

APPENDIX (cont.)

Sample NC083-35. Cadia Intrusive Complex, Cadia Quarry quartz monzonite porphyry
Drill hole NC083, depth 35.0 m, AMG coordinates (AGD84 datum), 685092E, 6296855N

	Zircon analyses						Total				Radiogenic		Age (Ma)	
Grain spot	U (ppm)	Th (ppm)	Th/U	$^{206}Pb^*$ (ppm)	$^{204}Pb/^{206}Pb$	f_{206} %	$^{238}U/^{206}Pb$	±1σ	$^{207}Pb/^{206}Pb$	±1σ	$^{206}Pb/^{238}U$	±1σ	$^{206}Pb/^{238}U$	±1σ
1.1	210	60	0.29	12.8	0.000138	0.29	14.08	0.16	0.0580	0.0008	0.0708	0.0008	441.1	4.8
2.1	180	54	0.30	11.5	0.000088	0.11	13.47	0.15	0.0571	0.0009	0.0742	0.0008	461.2	4.9
3.1	334	102	0.31	21.3	0.000183	0.05	13.43	0.25	0.0567	0.0006	0.0744	0.0014	462.6	8.3
3.2	293	141	0.48	18.5	0.000017	0.09	13.59	0.14	0.0568	0.0007	0.0735	0.0007	457.3	4.5
4.1	269	123	0.46	15.6	-	0.15	14.83	0.16	0.0564	0.0007	0.0673	0.0007	420.1	4.3
5.1	111	36	0.33	7.0	-	0.02	13.68	0.18	0.0562	0.0011	0.0731	0.0010	454.6	5.8
6.1	182	64	0.35	10.8	-	0.15	14.44	0.15	0.0567	0.0008	0.0691	0.0007	431.0	4.5
7.1	319	173	0.54	19.0	0.000051	0.16	14.42	0.15	0.0568	0.0006	0.0692	0.0007	431.6	4.4
7.2	251	98	0.39	15.6	0.000174	0.30	13.78	0.21	0.0584	0.0007	0.0724	0.0011	450.3	6.6
8.1	345	155	0.45	21.0	0.000122	<0.01	14.12	0.13	0.0557	0.0005	0.0708	0.0007	441.2	4.1
9.1	228	78	0.34	14.6	0.000243	0.07	13.46	0.15	0.0568	0.0006	0.0742	0.0008	461.7	5.1
9.2	273	96	0.35	17.5	-	<0.01	13.42	0.13	0.0559	0.0006	0.0746	0.0007	463.6	4.5
*10.1	227	86	0.38	15.3	0.000243	0.06	12.74	0.15	0.0573	0.0006	0.0784	0.0010	486.8	5.8
11.1	194	52	0.27	12.0	0.000170	0.07	13.89	0.14	0.0565	0.0007	0.0720	0.0007	447.9	4.3
12.1	116	34	0.29	6.9	0.000229	0.27	14.53	0.16	0.0576	0.0009	0.0686	0.0008	427.9	4.7
12.2	196	88	0.45	12.3	0.000164	0.10	13.68	0.14	0.0569	0.0007	0.0730	0.0007	454.3	4.4
13.1	262	100	0.38	15.6	0.000073	0.13	14.44	0.14	0.0565	0.0006	0.0692	0.0007	431.2	4.0
14.1	208	73	0.35	12.4	0.000153	0.23	14.39	0.16	0.0574	0.0006	0.0693	0.0008	432.0	4.7
15.1	181	54	0.30	11.3	0.000179	0.04	13.79	0.18	0.0563	0.0009	0.0725	0.0010	451.0	5.9
16.1	363	151	0.42	21.6	0.000123	0.21	14.47	0.13	0.0571	0.0005	0.0689	0.0006	429.8	3.8
17.1	278	135	0.49	16.7	0.000068	0.12	14.26	0.18	0.0566	0.0005	0.0700	0.0009	436.5	5.4
*excluded spot		Older population, 10 spots					MSWD = 1.20				Weighted mean		456.4	5.1
		Younger population, 10 spots					MSWD = 1.05				Weighted mean		429.7	4.2

Sample NC486-467. Cadia Intrusive Complex, Cadia Quarry quartz monzonite porphyry
Drill hole NC486, depth 467.0 m, AMG coordinates (AGD84 datum), 685001E, 6296883N

	Zircon analyses						Total				Radiogenic		Age (Ma)	
Grain spot	U (ppm)	Th (ppm)	Th/U	$^{206}Pb^*$ (ppm)	$^{204}Pb/^{206}Pb$	f_{206} %	$^{238}U/^{206}Pb$	±1σ	$^{207}Pb/^{206}Pb$	±1σ	$^{206}Pb/^{238}U$	±1σ	$^{206}Pb/^{238}U$	±1σ
1.1	135	39	0.29	8.3	0.000457	0.29	14.057	0.187	0.0581	0.0012	0.0709	0.0010	441.8	5.8
2.1	252	72	0.28	15.2	0.000054	0.18	14.269	0.173	0.0571	0.0009	0.0700	0.0009	435.9	5.2
3.1	217	76	0.35	13.6	0.000332	0.24	13.747	0.169	0.0579	0.0010	0.0726	0.0009	451.6	5.5
4.1	613	295	0.48	38.4	0.000381	0.73	13.696	0.147	0.0619	0.0010	0.0725	0.0008	451.1	4.8
5.1	160	47	0.30	9.8	0.000299	0.54	14.117	0.210	0.0601	0.0013	0.0705	0.0011	438.9	6.5
6.1	422	182	0.43	26.3	0.000133	0.00	13.762	0.327	0.0560	0.0008	0.0727	0.0018	452.2	10.5
7.1	179	83	0.46	11.3	0.000189	0.18	13.659	0.171	0.0575	0.0015	0.0731	0.0009	454.7	5.6
8.1	218	107	0.49	13.9	0.000082	0.27	13.449	0.164	0.0584	0.0010	0.0742	0.0009	461.1	5.5
9.1	119	40	0.34	7.2	-	0.51	14.240	0.288	0.0597	0.0022	0.0699	0.0014	435.3	8.7
10.1	288	136	0.47	17.5	0.000106	<0.01	14.140	0.225	0.0557	0.0009	0.0707	0.0011	440.5	6.9
11.1	327	149	0.46	19.8	0.000027	0.19	14.156	0.167	0.0572	0.0009	0.0705	0.0008	439.2	5.1
12.1	265	71	0.27	16.5	-	0.23	13.735	0.171	0.0578	0.0010	0.0726	0.0009	452.1	5.5
13.1	175	66	0.38	10.9	-	0.28	13.711	0.213	0.0583	0.0013	0.0727	0.0012	452.6	6.9
14.1	223	88	0.40	14.0	-	0.36	13.676	0.174	0.0589	0.0011	0.0729	0.0009	453.4	5.7
15.1	306	134	0.44	19.2	0.000196	0.31	13.683	0.167	0.0585	0.0009	0.0729	0.0009	453.4	5.4
16.1	221	78	0.35	13.7	0.000210	0.33	13.827	0.170	0.0586	0.0010	0.0721	0.0009	448.7	5.4
17.1	131	40	0.30	7.9	0.000143	0.20	14.186	0.199	0.0573	0.0014	0.0704	0.0010	438.3	6.1
18.1	155	47	0.30	9.6	0.000205	0.34	13.797	0.224	0.0587	0.0013	0.0722	0.0012	449.6	7.2
19.1	155	51	0.33	9.9	0.000524	0.17	13.508	0.185	0.0576	0.0013	0.0739	0.0010	459.6	6.2
*20.1	132	40	0.31	7.7	0.000136	0.29	14.752	0.208	0.0576	0.0014	0.0676	0.0010	421.6	5.9
*excluded spot		Older population, 12 spots					MSWD = 0.41				Weighted mean		453.4	4.3
		Younger population, 7 spots					MSWD = 0.13				Weighted mean		438.7	5.1

APPENDIX (cont.)

Sample NC486-608. Cadia Intrusive Complex, Cadia Quarry quartz monzonite porphyry
Drill hole NC486, depth 608.0 m, AMG cCoordinates (AGD84 datum), 685074E, 6296953N

	Zircon analyses						Total				Radiogenic		Age (Ma)	
Grain spot	U (ppm)	Th (ppm)	Th/U	$^{206}Pb^*$ (ppm)	$^{204}Pb/^{206}Pb$	f_{206} %	$^{238}U/^{206}Pb$	±1σ	$^{207}Pb/^{206}Pb$	±1σ	$^{206}Pb/^{238}U$	±1σ	$^{206}Pb/^{238}U$	±1σ
1.1	128	39	0.31	7.9	0.000191	0.31	13.968	0.189	0.0583	0.0013	0.0714	0.0010	444.4	5.9
2.1	189	63	0.33	11.4	0.000058	<0.01	14.290	0.216	0.0551	0.0010	0.0700	0.0011	436.3	6.5
3.1	284	93	0.33	17.1	0.000100	0.27	14.311	0.170	0.0578	0.0010	0.0697	0.0008	434.3	5.1
4.1	421	98	0.23	25.4	-	0.02	14.228	0.160	0.0558	0.0007	0.0703	0.0008	437.8	4.8
5.1	764	393	0.51	46.7	-	<0.01	14.062	0.150	0.0557	0.0005	0.0711	0.0008	442.9	4.6
6.1	215	78	0.36	13.2	-	0.05	13.998	0.174	0.0562	0.0011	0.0714	0.0009	444.6	5.4
7.1	370	160	0.43	22.2	0.000000	0.04	14.338	0.166	0.0559	0.0010	0.0697	0.0008	434.5	5.0
8.1	224	101	0.45	13.6	0.000181	0.13	14.178	0.236	0.0567	0.0011	0.0704	0.0012	438.8	7.2
9.1	243	117	0.48	14.4	0.000094	0.27	14.512	0.177	0.0576	0.0011	0.0687	0.0009	428.5	5.1
10.1	251	80	0.32	15.2	-	0.35	14.213	0.170	0.0585	0.0010	0.0701	0.0009	436.8	5.2
11.1	205	72	0.35	12.5	-	0.44	14.057	0.220	0.0593	0.0011	0.0708	0.0011	441.2	6.8
*12.1	245	82	0.34	15.3	-	0.07	13.778	0.190	0.0566	0.0010	0.0725	0.0010	451.4	6.1
13.1	216	105	0.49	13.0	0.000025	0.38	14.322	0.177	0.0586	0.0011	0.0696	0.0009	433.5	5.3
14.1	274	118	0.43	16.6	0.000185	0.13	14.179	0.166	0.0567	0.0009	0.0704	0.0008	438.8	5.0
15.1	226	60	0.27	13.6	-	0.22	14.235	0.208	0.0574	0.0012	0.0701	0.0010	436.7	6.3
16.1	246	80	0.33	14.9	0.000119	<0.01	14.194	0.174	0.0551	0.0010	0.0705	0.0009	439.2	5.3
17.1	317	143	0.45	18.8	0.000139	0.32	14.541	0.169	0.0580	0.0009	0.0686	0.0008	427.4	4.9
18.1	565	365	0.65	33.3	0.000226	0.20	14.592	0.183	0.0569	0.0007	0.0684	0.0009	426.5	5.3
19.1	195	48	0.25	11.7	-	0.05	14.343	0.188	0.0559	0.0011	0.0697	0.0009	434.3	5.6
20.1	203	65	0.32	12.5	0.000186	0.52	13.937	0.211	0.0601	0.0013	0.0714	0.0011	444.4	6.6
*excluded spot		Single population, 19 spots					MSWD = 1.05				Weighted mean		436.5	3.5

Sample NC384-200. Cadia Intrusive Complex, Cadia Hill quartz monzonite porphyry
Drill hole NC384, depth 200.0 m, AMG coordinates (AGD84 datum), 685330E, 6296060N

	Zircon analyses						Total				Radiogenic		Age (Ma)	
Grain spot	U (ppm)	Th (ppm)	Th/U	$^{206}Pb^*$ (ppm)	$^{204}Pb/^{206}Pb$	f_{206} %	$^{238}U/^{206}Pb$	±1σ	$^{207}Pb/^{206}Pb$	±1σ	$^{206}Pb/^{238}U$	±1σ	$^{206}Pb/^{238}U$	±1σ
*1.1	230	78	0.34	14.3	-	0.05	13.782	0.166	0.0564	0.0010	0.0725	0.0009	451.3	5.3
*2.1	180	58	0.32	10.6	0.000018	0.60	14.578	0.218	0.0601	0.0011	0.0682	0.0010	425.2	6.3
*3.1	237	115	0.48	13.9	0.000793	0.94	14.645	0.218	0.0628	0.0010	0.0676	0.0010	421.9	6.2
4.1	133	40	0.30	8.1	0.000282	0.11	14.055	0.193	0.0567	0.0013	0.0711	0.0010	442.6	6.0
5.1	145	43	0.29	8.7	-	0.21	14.277	0.192	0.0572	0.0013	0.0699	0.0010	435.5	5.8
6.1	208	70	0.34	12.6	-	0.09	14.216	0.238	0.0564	0.0016	0.0703	0.0012	437.8	7.2
7.1	325	170	0.52	19.4	0.000378	0.09	14.397	0.169	0.0562	0.0009	0.0694	0.0008	432.5	5.0
8.1	260	133	0.51	15.8	0.000035	<0.01	14.128	0.208	0.0557	0.0015	0.0708	0.0011	440.9	6.4
9.1	2227	1636	0.73	136.6	0.000362	0.75	14.002	0.165	0.0618	0.0005	0.0709	0.0009	441.4	5.1
10.1	333	158	0.47	19.8	0.000172	0.21	14.455	0.166	0.0571	0.0008	0.0690	0.0008	430.3	4.9
11.1	154	49	0.32	9.1	0.000539	0.13	14.519	0.194	0.0565	0.0012	0.0688	0.0009	428.8	5.7
12.1	1658	1645	0.99	100.8	0.000018	0.09	14.127	0.169	0.0564	0.0004	0.0707	0.0009	440.5	5.2
13.1	172	45	0.26	10.4	0.000310	0.19	14.248	0.184	0.0571	0.0012	0.0701	0.0009	436.5	5.6
14.1	277	98	0.35	16.6	-	0.18	14.381	0.171	0.0570	0.0009	0.0694	0.0008	432.6	5.1
15.1	143	40	0.28	8.5	0.000072	0.02	14.447	0.193	0.0556	0.0013	0.0692	0.0009	431.4	5.7
16.1	117	38	0.32	7.2	-	0.11	14.039	0.200	0.0567	0.0015	0.0712	0.0010	443.1	6.2
*17.1	310	72	0.23	19.3	0.000272	0.03	13.761	0.162	0.0562	0.0009	0.0726	0.0009	452.1	5.2
18.1	339	159	0.47	20.6	-	0.11	14.094	0.183	0.0566	0.0008	0.0709	0.0009	441.4	5.6
19.1	272	90	0.33	16.2	0.000118	0.31	14.451	0.210	0.0580	0.0016	0.0690	0.0010	430.0	6.2
20.1	149	42	0.28	8.9	-	0.04	14.430	0.262	0.0558	0.0012	0.0693	0.0013	431.8	7.7
*excluded spots		Single population, 16 spots					MSWD = 0.78				Weighted mean		435.9	3.7

APPENDIX (cont.)

Sample NC475-1247. Cadia Intrusive Complex, Cadia East quartz monzonite porphyry
Drill hole NC475, depth 1247.0 m, AMG coordinates (AGD84 datum), 686179E, 6295919N

	Zircon analyses						Total				Radiogenic		Age (Ma)	
Grain spot	U (ppm)	Th (ppm)	Th/U	$^{206}Pb^*$ (ppm)	$^{204}Pb/^{206}Pb$	f_{206} %	$^{238}U/^{206}Pb$	±1σ	$^{207}Pb/^{206}Pb$	±1σ	$^{206}Pb/^{238}U$	±1σ	$^{206}Pb/^{238}U$	±1σ
*1.1	1541	937	0.61	93	0.000002	<0.01	14.213	0.153	0.0554	0.0004	0.0704	0.0008	438.5	4.6
2.1	1160	691	0.60	72	0.000023	0.01	13.845	0.144	0.0560	0.0004	0.0722	0.0008	449.5	4.6
3.1	998	998	1.00	61	0.000045	0.09	14.088	0.148	0.0564	0.0006	0.0709	0.0008	441.7	4.5
4.1	1570	942	0.60	99	0.000020	0.05	13.606	0.149	0.0565	0.0004	0.0735	0.0008	457.0	4.9
5.1	2031	1672	0.82	126	0.000030	0.01	13.875	0.141	0.0560	0.0003	0.0721	0.0007	448.6	4.5
*6.2	1276	1122	0.88	77	-	0.10	14.143	0.147	0.0565	0.0004	0.0706	0.0007	440.0	4.5
6.1	1663	1003	0.60	105	-	0.03	13.627	0.160	0.0563	0.0004	0.0734	0.0009	456.4	5.3
7.1	2545	2499	0.98	161	0.000043	<0.01	13.596	0.147	0.0558	0.0003	0.0736	0.0008	457.7	4.8
8.1	2677	2600	0.97	168	0.000008	0.02	13.719	0.143	0.0562	0.0003	0.0729	0.0008	453.4	4.6
9.1	1295	1356	1.05	82	-	<0.01	13.548	0.140	0.0555	0.0004	0.0739	0.0008	459.5	4.7
10.1	1305	803	0.62	82	0.000018	<0.01	13.741	0.163	0.0554	0.0004	0.0728	0.0009	453.2	5.3
11.1	969	673	0.70	60	0.000004	<0.01	13.787	0.145	0.0559	0.0005	0.0725	0.0008	451.4	4.6
*12.1	1823	1205	0.66	118	0.000067	<0.01	13.302	0.136	0.0562	0.0004	0.0752	0.0008	467.4	4.7
*13.1	1486	938	0.63	95	0.000030	<0.01	13.384	0.138	0.0556	0.0004	0.0748	0.0008	464.9	4.7
*14.1	858	531	0.62	52	-	0.09	14.277	0.153	0.0563	0.0005	0.0700	0.0008	436.0	4.6
15.1	1062	648	0.61	65	-	0.08	14.009	0.146	0.0564	0.0004	0.0713	0.0008	444.1	4.5
16.1	1188	853	0.72	74	0.000024	0.15	13.825	0.144	0.0572	0.0004	0.0722	0.0008	449.5	4.6
17.1	1026	847	0.83	64	0.000017	0.13	13.759	0.145	0.0570	0.0005	0.0726	0.0008	451.7	4.7
18.1	525	304	0.58	32	-	0.07	13.942	0.153	0.0564	0.0006	0.0717	0.0008	446.2	4.8
*19.1	730	487	0.67	44	0.000117	0.01	14.335	0.153	0.0557	0.0005	0.0698	0.0008	434.7	4.6
*excluded spots		Single population, 14 spots					MSWD = 1.20				Weighted mean		451.0	1.4

Notes: f_{206}% denotes the percentage of ^{206}Pb that is common Pb; correction for common Pb made using the measured $^{238}U/^{206}Pb$ and $^{207}Pb/^{206}Pb$ ratios following Tera and Wasserburg (1972) as outlined in Compston et al. (1992)